THE PENNSYLVANIA STATE UNIVERSITY
SCHREYER HONORS COLLEGE

DEPARTMENT OF ASTRONOMY & ASTROPHYSICS

NEID REVEALS THAT THE YOUNG WARM NEPTUNE TOI-2076 b HAS A LOW OBLIQUITY

ROBERT C. FRAZIER
SPRING 2023

A thesis
submitted in partial fulfillment
of the requirements
for baccalaureate degrees
in Astronomy & Astrophysics and Physics
with honors in Astronomy & Astrophysics

Reviewed and approved* by the following:

Suvrath Mahadevan
Professor of Astronomy & Astrophysics
Thesis Supervisor

Jane Charlton
Professor of Astronomy & Astrophysics
Honors Adviser

*Signatures are on file in the Schreyer Honors College.

Abstract

TOI-2076 b is a sub-Neptune-sized planet ($R = 2.39 \pm 0.10\,\mathrm{R}_\oplus$) that transits a young ($204 \pm 50\,\mathrm{MYr}$) bright ($V = 9.2$) K-dwarf hosting a system of three transiting planets. Using spectroscopic observations with the NEID spectrograph on the WIYN 3.5 m Telescope, I model the Rossiter-McLaughlin effect of TOI-2076 b, and derive a sky-projected obliquity of $\lambda = -3^{+16\,\circ}_{-15}$. Using the size of the star ($R = 0.775 \pm 0.015\,\mathrm{R}_\odot$), and the stellar rotation period ($P_{\mathrm{rot}} = 7.27 \pm 0.23$ days), I estimate an obliquity of $\psi = 18^{+10\,\circ}_{-9}$ ($\psi < 34^\circ$ at 95% confidence), demonstrating that TOI-2076 b is on a well-aligned orbit. Simultaneous diffuser-assisted photometry from the 3.5 m Telescope at Apache Point Observatory rules out flares during the transit. TOI-2076 b joins a small but growing sample of young planets in compact multi-planet systems with well-aligned orbits, and is the fourth planet with an age $\lesssim 300$ Myr in a multi-transiting system with an obliquity measurement. The low obliquity of TOI-2076 b and the presence of transit timing variations in the system suggest the TOI-2076 system likely formed via convergent disk migration in an initially well-aligned disk.

Table of Contents

List of Figures

List of Tables

Acknowledgements

I would like to extend my deepest thanks to Dr. Suvrath Mahadevan who supported and guided me throughout this project as my thesis and research advisor. Without him I would not have been able to do this project (or learn the importance of group meetings and deadlines).

Dr. Guðmundur Stefánsson from Princeton University was integral to this project, he provided me with consistent support, guidance, and instruction that let me start and continue with this project. He has helped me understand the process of research, review, and revision, and overall, helped me become a better researcher.

I would also like to extend overall thanks to the NEID team and Professor Mahadevan's research group for providing me assistance and feedback during the research and paper writing process. Also, thank you to them, and Professor Mahadevan, for creating such a welcoming and supportive environment.

Last, but never least, thank you to my friends and family for supporting me throughout all of college, without them I would not have made it this far.

This work was performed for the Jet Propulsion Laboratory, California Institute of Technology, sponsored by the United States Government under the Prime Contract 80NM0018D0004 between Caltech and NASA. We acknowledge support from NSF grants AST-1909506, AST-190950, AST-1910954, AST-1907622, and AST-1907622, and the Research Corporation for precision photometric observations with diffuser-assisted photometry.

Data presented were obtained by the NEID spectrograph built by Penn State University and operated at the WIYN Observatory by NOIRLab, under the NN-EXPLORE partnership of the National Aeronautics and Space Administration and the National Science Foundation.

The findings and conclusions of this paper do not necessarily reflect the view of the funding agencies that supported this work.

Chapter 1

Introduction

The research presented in this thesis is also published in Frazier et al. (2023). This publication was a result entirely of the research conducted as part of this thesis. Therefore it is natural that significant text and figure overlap exists between this published paper and this thesis.

Stellar obliquity—the angle between the stellar rotation axis and the planet orbital axis—is a powerful probe of the dynamical formation histories of planetary systems (Albrecht et al., 2022). Stellar obliquities have most successfully been measured with the Rossiter-McLaughlin (RM) Effect (Rossiter, 1924; McLaughlin, 1924), which relies on measuring spectral line distortions approximated as radial velocity (RV) shifts during as a companion transits the host star. As the star rotates on its axis, light emitted from the part rotating towards the observer is blueshifted and light emitted from the part rotating away from the observer is redshifted. This results in spectral line broadening. As the planet transits across the star, it blocks out part of the light from either the blueshifted or redshifted section of the star, weakening that Doppler shifted part of the star's impact on the spectral line broadening. This is generally interpreted as net shifts in the radial velocity observed from the star. RM measurements made over the last two decades have revealed a broad distribution of sky-projected obliquities, λ, from well-aligned to highly misaligned systems (see Albrecht et al., 2022, and references therein).

However, the RM effect is primarily sensitive to the sky projection of the obliquity, λ, rather than the true 3D angle between the stellar rotation axis and the planet orbital axis, ψ[1]. When the sky projection of the obliquity λ is combined with knowledge of the stellar inclination, $i_\star$, and the orbital inclination of the planet, the 3D obliquity ψ can be estimated. Recently, through constructing a sample of 3D obliquities, Albrecht et al. (2021) revealed a possible exoplanet architectural dichotomy, where hot Jupiters are primarily seen to orbit on either well-aligned orbits, or on close to polar orbits. However, the sample from Albrecht et al. (2021) is dominated by hot Jupiters—as such planets are the easiest to measure with RVs due to their massive size and close in orbits—and it is unclear if this reflects a property intrinsic to only how hot Jupiters form, or if this dichotomy

[1] In the special case where the differential rotation is known or can be measured the RM effect can place a constraint on the three-dimensional obliquity (see e.g., Gaudi and Winn, 2007; Sasaki and Suto, 2021).

is more broadly seen for other types of planetary systems.

Next-generation RV spectrographs are capable of measuring the obliquities of smaller planets, and the growing sample of smaller planets with obliquity measurements hints that the dichotomy might also be seen for such planets (Stefánsson et al., 2022). However, additional observations are needed to increase the size of the small sample ($\lesssim$10). In this context, observations of low-mass planets ($\lesssim 0.3\,\mathrm{M_J}$) in young systems ($< 1\,\mathrm{Gyr}$) with precisely determined ages are particularly valuable, as they can help yield insights into the possible timescales involved in the different processes that are invoked to excite obliquities—such as planet-planet scattering (Rasio and Ford, 1996), Von Zeipel-Lidov-Kozai oscillations (e.g., Fabrycky and Tremaine, 2007; Naoz, 2016), or secular resonance crossings with a disappearing disk and a massive outer companion (Petrovich et al., 2020)—or dampen them through tidal interactions (see discussion in Albrecht et al., 2012). Planet-planet scattering relies on planets orbits bringing them close to each other, and the resulting gravitational interaction (and possible collision between the planets) causes their orbits to become eccentric and misaligned (Rasio and Ford, 1996). Von Zeipel-Lidov-Kozai oscillations occur when the a tight binary system is periodically perturbed by a distant eccentric or misaligned third body (planet or star), causing oscillations in the system's obliquity and eccentricity (Fabrycky and Tremaine, 2007; Naoz, 2016). Secular resonance crossing occurs as an inner planet's and a larger outer planet's procession frequency may align as the protoplanetary disk disperses, causing the inner planet to become misaligned (Petrovich et al., 2020). All of these processes occur on different timescales, with planet-planet scattering potentially taking as little as thousands of years while Von Zeipel-Lidov-Kozai oscillations take millions of years.

To conduct precise obliquity measurements of small planets, extremely precise radial velocity (EPRV) instruments are needed. These next-generation RV spectrographs obtain sub 1 m/s precision and include NEID (Schwab et al., 2016; Halverson et al., 2016), EXPRES (Jurgenson et al., 2016), ESPRESSO (Pepe et al., 2021), HARP-N (Cosentino et al., 2012), and MAROON-X (Seifahrt et al., 2018). Beyond obliquity measurements, EPRV measurements are the path forward for detecting small and long-period planets, including the detectiong of true Earth analogues. An

Earth-mass planet orbiting around a Sun-like star with a 1 year orbital period would produce a reflex radial velocity of 9 cm/s (Crass et al., 2021). This level of precision requires not just incredible precision at the instrument level, but also disentangling the effects of stellar variability and activity that become dominant at this small scale. The 2018 National Academy Exoplanet Science Strategy report and the 2010 Astronomy and Astrophysics Decadal Survey have recommended furthering the development of EPRV measurements for finding other Earths (Crass et al., 2021), especially to support future Next Great Observatory concepts such as the Large Ultraviolet Optical Infrared Surveyor (LUVOIR; Team (2019)) and the Habitable Exoplanet Observatory (HabEx; Gaudi et al. (2020)). To this end, NASA and NSF have created the Extreme Precision Radial Velocity Working Group (Crass et al., 2021) which produced a fifteen year road map for a development program to reach consistent EPRV measurements for finding Earth analogs. While the focus is on radial velocity detection of exoplanets, these improvements will also allow for obliquity measurements of smaller and longer period planets.

In this paper, I measure the stellar obliquity of TOI-2076 b, a warm sub-Neptune transiting a young ($204 \pm 50\,\mathrm{MYr}$; Osborn et al., 2022) and active K-dwarf. The TOI-2076 planetary system—which hosts at least three transiting planets—was discovered by Hedges et al. (2021) using two sectors of photometric data from the Transiting Exoplanet Survey Satellite (TESS; Ricker et al., 2015). The system was further studied by Osborn et al. (2022) using the same two sectors in combination with data from the CHEOPS satellite (Benz et al., 2021), and revealed Transit Timing Variations (TTVs) at the $\sim$10 min level. The known planets in the system have orbital periods of $P_b = 10.4\,\mathrm{days}$, $P_c = 21.0\,\mathrm{days}$, and $P_d = 35.1\,\mathrm{days}$, and radii of $R_b = 2.5\,\mathrm{R}_\oplus$, $R_c = 3.5\,\mathrm{R}_\oplus$ and $R_d = 3.2\,\mathrm{R}_\oplus$), for planets b, c, and d, respectively (Osborn et al., 2022). Further, Zhang et al. (2023) recently claim evidence of He 10830Å absorption during the transit of TOI-2076 b, suggesting that the atmosphere is experiencing atmospheric evaporation, though with additional observations Gaidos et al. (2023) caution that the absorption signature is most likely due to variability of the Helium line due to stellar activity of the young star.

To constrain the obliquity of TOI-2076 b, spectroscopic in-transit observations were obtained

using the Penn State built NEID spectrograph (Schwab et al., 2016; Halverson et al., 2016) on the WIYN 3.5m Telescope at Kitt Peak National Observatory, which demonstrate that TOI-2076 b is on a well-aligned orbit. In addition, diffuser-assisted photometry using the Engineered Diffuser on the ARC 3.5 m Telescope at Apache Point Observatory (APO) reveal no flare events during transit that otherwise could complicate the RM analysis. TOI-2076 b joins a growing sample of warm Neptunes orbiting young stars on well-aligned orbits.

Chapter 2

Observations

2.1 TESS

The Transiting Exoplanet Survey Satellite (TESS; Ricker et al., 2015), launched in 2018 as a NASA Astrophysics Explorer mission, observed TOI-2076 in three sectors: Sector 16 (September 12 to October 6 2019), Sector 23 (March 19 to April 15 2020), and Sector 50 (March 26 to April 22 2022) with the TESS two-minute cadence. In comparison to the earlier Kepler mission, TESS observes the whole night-sky versus a specific section (TESS' viewing area is 400 times larger than Kepler's) and it looks at stars about 10 to 100 times brighter than Kepler did. TESS focuses on searching for exoplanets around nearby bright stars, these planets are more amenable to follow-up observations for confirmation and characterization. Its goal in the first two years of observation was to look at at least 200,000 main sequence dwarf stars and find more than 1000 planets smaller than Neptune. TESS uses four CCD cameras to observe in the 600 nm to 1000 nm range, each with a 24×24 deg field of view, resulting in a combined 24×96 deg field of view. It observes preselected targets (such as TOI-2076) at a two minute cadence as well as taking 30 minute cadence full frame images. TESS, to date, has observed a total of 57 sectors with 6133 objects of interest observed, 1346 of these with radii $< 4\,\mathrm{R}_\oplus$ (fulfilling its goal of more than 1000 sub-Neptune defections), and a total of 282 confirmed planets (Center, 2022). The TESS data is processed by the Science Processing Operations Center (SPOC; Jenkins et al., 2016) which removes systematic errors, and extracts the photometry, before being being released publicly. I retrieved the SPOC photometric data of TOI-2076 using the `lightkurve` (Lightkurve Collaboration et al., 2018) package. The Presearch Data Conditioning Single Aperture Photometry (PDCSAP) lightcurve, which contains systematics-corrected data using the algorithms originally developed for the *Kepler* data analysis pipeline, was analyzed. 12,495 data points with TESS non-zero quality flags (e.g., due to guiding issues, excess stray light) were removed, leaving 38,950 data points for subsequent analysis.

2.2 NEID

A transit of TOI-2076 b was observed with the NEID spectrograph (Schwab et al., 2016) on the WIYN 3.5m telescope at Kitt Peak Observatory[1] NEID is an environmentally stabilized (Robertson et al., 2019) fiber-fed high ($R \sim 113,000$) resolution spectrograph covering a broad wavelength range from $380 - 930\,\mathrm{nm}$ with a designed instrumental precision of 27 cm/s (Halverson et al., 2016). It was built as part of the NASA-NSF Exoplanet Observational Research (NN-Explore) initiative to provide an extremely precise radial velocity instrument for the 3.5m WIYN telescope for the purpose of providing mass constraints on Earth-mass planets in the habitable zone. In this function, it works in conjunction with transiting planet hunters such as TESS. It is also engaged in the NEID Earth Twin Survey (NETS) which looks to find previously undetected Earth-like exoplanets around nearby bright stars (Gupta and Schlichting, 2019).

The transit was observed on the night of 13 Feb 2022 for 5.5 hours. In total, using an exposure time of $600\,\mathrm{s}$, 33 spectra spanning a period of 1 hour before and after the 3.3 hour transit (Hedges et al., 2021) were obtained. The resulting median signal to noise ratio was 105.1 at 5500 Å. The target rose from airmass 1.90 to 1.02 during the observation.

The NEID spectra were processed with the NEID Data Reduction Pipeline (DRP)[2].The RVs were extracted with a custom version of the Spectrum Radial Velocity Analyzer (SERVAL; Zechmeister et al., 2018) that has been adapted and optimized for NEID data (see Stefánsson et al., 2022). using all of the available NEID spectra to generate the template for the RV calculation with SERVAL[3]. SERVAL generates a master template from all observed spectra and determines the RV shifts by minimizing the χ^2 statistic between the master template and the individual observed spectra. Barrycentric corrections are made using the `barrycorrpy` package (Kanodia and Wright, 2018) which is based on algorithms from Wright & Eastman 2014. Telluric masking was done

[1]WIYN is a joint facility of the University of Wisconsin–Madison, Indiana University, NSF's NOIRLab, the Pennsylvania State University, Purdue University, University of California, Irvine, and the University of Missouri.

[2]`https://neid.ipac.caltech.edu/docs/NEID-DRP/`

[3]We experimented creating a template using derived only from spectra outside of the transit window. Doing so resulted in fully consistent RVs with only a 10cm/s RMS difference between the two different extractions.

using `telfit` (Gullikson et al., 2014), a Python wrapper for the Line-by-Line Radiative Transfer Model package (`LBLRTM`; Clough et al. (2005)), to generate the telluric mask. The resulting radial velocities agree well with the RVs from the NEID DRP derived with the cross-correlation functions (CCF) method; the median RV error from the SERVAL pipeline is $0.88\,\mathrm{m/s}$ and it is $1.5\,\mathrm{m/s}$ from the CCF method. I elected to use the SERVAL RVs given their higher RV precision. The RV observations show a feature consistent with the RM effect as well as an upward RV trend that I explore in detail in Section 4.

2.3 Diffuser-assisted Photometry

During the spectroscopic transit, simultaneous photometry was obtained using the Engineered Diffuser (Stefansson et al., 2017) available on the Astrophysical Research Council Telescope Imaging Camera (ARCTIC) instrument (Huehnerhoff et al., 2016) on the ARC 3.5 m Telescope at Apache Point Observatory. To obtain high precision observations of the bright star, the Engineered Diffuser, which spreads out the light of the star in a well-defined top-hat shape (Stefansson et al., 2017) while maintaining a stable PSF throughout the observations, was used. The transit was observed using the SDSS i' filter with a short exposure time of 8 seconds due to the brightness of the host star. ARCTIC's 2×2 binning mode was used, resulting in a gain of 2.0 e/ADU and a plate scale of $0.22''/\mathrm{pixel}$. The target rose from airmass 1.72 to 1.01 during the observations. Wispy clouds during observation caused transparency fluctuations throughout the observations, which impacted the photometry.

To extract the photometry from the ARCTIC data, I used the AstroImageJ (Collins et al., 2017) software following the procedures in Stefansson et al. (2017), including bias and flat-field corrections. Prior to final aperture selection and analysis of the photometry, I used the `astroscrappy` (McCully et al., 2018) code to correct for cosmic rays and other charged particle events. I experimented with using a number of different apertures. For the final light curve analyzed in this work, I used an aperture size of 25 pixels (5.5") and sampled the background light with an annulus with

an inner radius of 45 pixels (9.9”) and an outer radius of 65 pixels (14.3”) around the star as this resulted in the lowest root mean square errors. The six reference stars that resulted in the smallest error in the transit model were all substantially fainter than the target, by about 230 times on average. The observations show a transit-like feature consistent with the expected depth and duration of the transit at the expected time, and reveal no large flares during the transit, which otherwise could complicate the RM analysis.

Chapter 3

Analysis

3.1 Stellar Parameters

Table 3.1 shows the parameters of the host star TOI-2076 used in this work. I adopt the stellar rotation period from Hedges et al. (2021), $P_{\rm rot} = 7.27 \pm 0.23\,{\rm days}$, which is precisely determined using long-term ground-based photometry from the Kilodegree Extremely Little Telescope (KELT; Pepper et al., 2007). As an additional measurement of the stellar rotation period, I used the `SpinSpotter` (Holcomb et al., 2022) code—which uses the autocorrelation function (ACF) to measure stellar rotation periods. Using `SpinSpotter` on the three available TESS sectors, I obtain a stellar rotation period of $P_{\rm rot} = 7.251 \pm 0.073\,{\rm days}$. This value is consistent with the value in Hedges et al. (2021), although the uncertainty from `SpinSpotter`—which is estimated as the standard deviation of the spacing between ACF vertexes—is underestimated.

To constrain the stellar spectroscopic parameters, the `SpecMatch-Emp`[1] (Yee et al., 2017) code—which constrains stellar spectroscopic parameters from comparing a spectrum of a star to a library of as-observed stars with well-constrained spectroscopic parameters— was used on the highest S/N NEID spectrum of TOI-2076 on segments of 100 Åbetween 5000 and 5800 Å. From the `SpecMatch-Emp` analysis, these values were obtained: $T_{\rm eff} = 5180 \pm 110\,{\rm K}$, [Fe/H]=$-0.01 \pm 0.09$, and $R_* = 0.79 \pm 0.08\,{\rm R}_\odot$. To constrain the projected rotational velocity of the star, the `SpecMatch-Synth`[2] code (Petigura, 2015), which compares the spectrum of a star to a library of theoretical spectra (Coelho et al., 2005) that can be artificially broadened to obtain estimates of $v \sin i$, was used. In doing so, the value $v \sin i = 5 \pm 1\,{\rm km/s}$ was obtained for TOI-2076. The uncertainties from these codes were internally calibrated using a "leave-one-out" procedure with the empirical library of well-characterized stars and observed spectra, and the uncertainties were found to be robust even at S/N as low as 20 per 1D extracted pixel. To obtain a model-dependent constraint on the mass and radius of the star, a spectral energy distribution (SED) fit was performed using the `SpecMatch-Emp` values and other available magnitudes and priors available from the literature using the `EXOFASTv2` code (Eastman et al., 2019) leveraging the Yonsei-Yale stellar

[1] `https://github.com/samuelyeewl/specmatch-emp`
[2] `https://github.com/petigura/specmatch-syn`

Table 3.1 Summary of stellar parameters used in this work.

Parameter	Description	Value	Notes
d	Distance	$41.963 \pm 0.028\,\mathrm{pc}$	(1)
P_{rot}	Stellar Rotation Period	$7.27 \pm 0.23\,\mathrm{days}$	(2)
Spectroscopic Parameters from the NEID spectra:			
T_{eff}	Effective Temperature	$5180 \pm 110\,\mathrm{K}$	(3)
[Fe/H]	Metallicity	-0.01 ± 0.09	(3)
R_*	Radius	$0.79 \pm 0.08\,\mathrm{R}_\odot$	(3)
$v \sin i$	Projected Rotational Velocity	$5 \pm 1\,\mathrm{km/s}$	(3)
Model-Dependent Stellar SED and Isochrone fit Parameters:			
M_*	Mass	$0.883 \pm 0.017\,\mathrm{M}_\odot$	(3)
R_*	Radius	$0.772^{+0.015}_{-0.016}\,\mathrm{R}_\odot$	(3)
ρ_*	Stellar Density	$2.720 \pm 0.165\,\mathrm{g/cm^3}$	(3)
T_{eff}	Effective Temperature	$5201^{+66}_{-61}\,\mathrm{K}$	(3)
Age	Age	$0.338^{+0.077}_{-0.081}\,\mathrm{Gyr}$	(3)
[Fe/H]	Metallicity	$0.017^{+0.077}_{-0.056}$	(3)
$\log g$	Surface Gravity in cgs units	4.608 ± 0.018	(3)

References are: (1) Gaia (Gaia Collaboration et al., 2021), (2) Hedges et al. (2021), (3) This work.

isochrone models. The final values are summarized in Table 3.1.

3.2 Photometric Analysis

To precisely constrain the orbital ephemerides of TOI-2076 b—important for the RM effect modeling—we utilized the `juliet` code (Espinoza et al., 2019) to perform a fit of the available TESS and diffuser-assisted APO transit photometry. As transit timing variations have been reported in the system with $\sim 10 - 15$ min amplitudes (Osborn et al., 2022; Zhang et al., 2023), I leveraged the functionality within `juliet` to account for TTVs by fitting the individual transit midpoints of the TESS transits and the APO transits separately. Our derived transit midpoints for TOI-2076 b are within 1σ with those reported in Osborn et al. (2022) and Zhang et al. (2023). For the fit, I used the `dynesty` dynamic nested sampler (Speagle, 2020) to sample the posteriors and the `batman` package (Kreidberg, 2015) to generate the light curve models. The priors and posteriors from the fit are summarized in Table 3.2. Figure 3.1 shows the TESS photometry along

Table 3.2 Summary of priors and resulting posteriors for the photometric analysis. $\mathcal{N}(m, \sigma)$ denotes a normal prior with mean m, and standard deviation σ; $\mathcal{U}(a, b)$ denotes a uniform prior with a start value a and end value b; and $J(a, b)$ denotes a log-uniform distribution between a lower limit a and an upper limit b.

Parameter	Description	Priors	Posteriors
Juliet Input Parameters:			
T_{TESS_0} $(\mathrm{BJD_{TDB}})$	Transit Midpoint, 1^{st} transit	$\mathcal{N}(2458743.7248, 0.042)$	$2458743.7183^{+0.0045}_{-0.0054}$
T_{TESS_1}	Transit Midpoint, 2^{nd} transit	$\mathcal{N}(2458754.080049, 0.042)$	$2458754.0768^{+0.0022}_{-0.0026}$
$T_{\mathrm{TESS}_{19}}$	Transit Midpoint, 20^{th} transit	$\mathcal{N}(2458940.474531, 0.042)$	$2458940.4810^{+0.0097}_{-0.0020}$
$T_{\mathrm{TESS}_{20}}$	Transit Midpoint, 21^{st} transit	$\mathcal{N}(2458950.82978, 0.042)$	$2458950.8343^{+0.0097}_{-0.0020}$
$T_{\mathrm{TESS}_{89}}$	Transit Midpoint, 90^{th} transit	$\mathcal{N}(2459665.341961, 0.042)$	$2459665.3542^{+0.0038}_{-0.0052}$
$T_{\mathrm{TESS}_{90}}$	Transit Midpoint, 91^{st} transit	$\mathcal{N}(2459675.69721, 0.042)$	$2459675.6942^{+0.0019}_{-0.0018}$
$T_{\mathrm{TESS}_{91}}$	Transit Midpoint, 92^{nd} transit	$\mathcal{N}(2459686.052459, 0.042)$	$2459686.0510^{+0.0014}_{-0.0013}$
$T_{\mathrm{APO}_{85}}$	Transit Midpoint, 86^{th} transit	$\mathcal{N}(2459623.920965, 0.042)$	$2459623.9183^{+0.0011}_{-0.0016}$
R_p/R_*	Radius ratio	$\mathcal{U}(0.0, 0.1)$	$0.0284^{+0.0011}_{-0.0010}$
e	Eccentricity	0.0	0.0
ω	Argument of periastron (°)	90.0	90.0
b	Impact parameter	$\mathcal{U}(0.0, 1.0)$	$0.123^{+0.077}_{-0.073}$
ρ	Stellar density (cgs)	$\mathcal{N}(2.720, 0.165)$	$2.712^{+0.099}_{-0.110}$
$q_{1\mathrm{TESS}}$	Linear limb darkening parameter	$\mathcal{U}(0.0, 1.0)$	$0.724^{+0.186}_{-0.230}$
$q_{2\mathrm{TESS}}$	Quadratic limb darkening parameter	$\mathcal{U}(0.0, 1.0)$	$0.463^{+0.227}_{-0.192}$
$M_{\mathrm{Dilution,TESS}}$	Dilution Factor	1.0	1.0
$M_{\mathrm{Flux,TESS}}$	Offset Relative Flux	$\mathcal{N}(0.0, 0.1)$	$-0.001^{+0.001}_{-0.001}$
$\sigma_{W\mathrm{TESS}}$	Jitter (ppm)	$\mathcal{J}(1.0, 5000.0)$	$140.7^{+5.1}_{-5.1}$
$q_{1\mathrm{APO}}$	Linear limb darkening parameter	$\mathcal{U}(0.0, 1.0)$	$0.196^{+0.170}_{-0.119}$
$q_{2\mathrm{APO}}$	Quadratic limb darkening parameter	$\mathcal{U}(0.0, 1.0)$	$0.602^{+0.256}_{-0.322}$
$M_{\mathrm{Dilution,APO}}$	Dilution Factor	1.0	1.0
$M_{\mathrm{Flux,APO}}$	Offset Relative Flux	$\mathcal{U}(0.0, 0.1)$	$0.00246^{+0.00026}_{-0.00024}$
$\sigma_{W\mathrm{APO}}$	Jitter (ppm)	$\mathcal{J}(1.0, 5000.0)$	$999.30^{+0.51}_{-1.02}$
Detrending Parameters:			
B_{TESS}	GP Amplitude	$\mathcal{J}(10^{-6}, 1.0)$	$0.000019^{+0.000008}_{-0.000005}$
C_{TESS}	GP Additive Factor	$\mathcal{J}(0.001, 1000.0)$	$0.014^{+0.058}_{-0.011}$
L_{TESS}	GP Length Scale (days)	$\mathcal{J}(0.0, 100000.0)$	$11.99^{+5.19}_{-3.10}$
P_{TESS}	GP Period (days)	$\mathcal{J}(2.0, 10.0)$	$4.01^{+0.17a}_{-0.16}$
$\theta_{0\mathrm{APO}}$	Linear Regressor Coefficient (APO airmass)	$\mathcal{U}(-100.0, 100.0)$	$0.002^{+0.002}_{-0.002}$
Derived Parameters:			
T_C $(\mathrm{BJD_{TDB}})$	Transit midpoint	-	$2458743.7247^{+0.0027}_{-0.0022}$
P	Orbital period (days)	-	$10.35527^{+0.00003}_{-0.00004}$
a/R_*	Scaled semi-major axis	-	$24.87^{+0.30}_{-0.33}$
i	Inclination (°)	-	$89.72^{+0.17}_{-0.18}$
S_{flux}	Insolation flux ($S_\oplus$)	-	$49.4^{+2.9}_{-2.7}$
T_{14}	Full transit duration (days)	-	$0.1352^{+0.0016}_{-0.0018}$
T_{23}	Interior transit duration (days)	-	$0.1275^{+0.0016}_{-0.0017}$
τ	Ingress time (days)	-	$0.0038^{+0.00017}_{-0.00016}$
R_p	Planetary radius ($R_\oplus$)	-	$2.39^{+0.10}_{-0.10}$
$T_{\mathrm{eq},a=0}$	Planet equilibrium temperature	-	738.0 ± 10.0

References are: (1) Gaia (Gaia Collaboration et al., 2021), (2) Hedges et al. (2021), (3) This work.

with the best-fit model and the phase-folded TESS photometry after accounting for the TTVs. The APO photometry and the best-fit model is shown in Figure 3.2.

To remove clear correlated noise signatures seen in the TESS data, I used the 'quasi-periodic' Gaussian Process kernel from the `celerite` package (Foreman-Mackey et al., 2017) available in `juliet`. Broad uninformative priors were placed on the GP hyper parameters. I note that the GP value $P_{TESS} = 4.01^{+0.17}_{-0.16}$ in Table 3.2 is different than our adopted value for stellar rotation period of $7.27 \pm 0.23\,\mathrm{days}$ as listed in Table 3.1. I attribute this difference being due to a combination of data gaps, and different spot evolution/behavior seen in the different TESS sectors. The latter two TESS sectors show faster time-scale variability than the first TESS sector, which I attribute to the young and active star likely having developed more spot complexes at different latitudes/longitudes. As noted in Section reftab:stellarparam, I adopt the $7.27 \pm 0.23\,\mathrm{days}$ value as the rotation period, as that value is derived from 8 years of ground-based monitoring as discussed in Hedges et al. (2021).

For the ground-based APO data, I observed a smooth trend during the observations. To remove the trend, I employed the linear detrending models available in `juliet`. I experimented detrending with a number of linear detrending parameters, including the airmass, X, and Y centroid coordinates, time etc. I found that a linear detrending using the airmass parameter yielded the highest quality fit measured from the residual scatter in the photometry after subtracting the detrended transit model from the data.

For the fit, I placed an informative Gaussian prior on the stellar density of $2.720 \pm 0.165\,\mathrm{g/cm^3}$ (see Table 3.1). I used the (q_1, q_2) limb-darkening parameterization as described in Kipping (2013). I experimented with a circular and an eccentric fit to model the photometry. Given that I only see a minimal statistical preference of $\Delta \ln(Z) = 0.42$ in favor of the eccentric model and that the posteriors between the two runs were within 1σ of each other (the eccentric model yielded a coarse constraint on $e = 0.28^{+0.37}_{-0.23}$ with $e < 0.77$ at 95% confidence), I elected to model the photometry assuming a circular orbit. This agrees with the approach of Hedges et al. (2021). Given the large $a/R_\star \sim 25$ for TOI-2076b, I acknowledge that it is a possibility that additional precise photometric

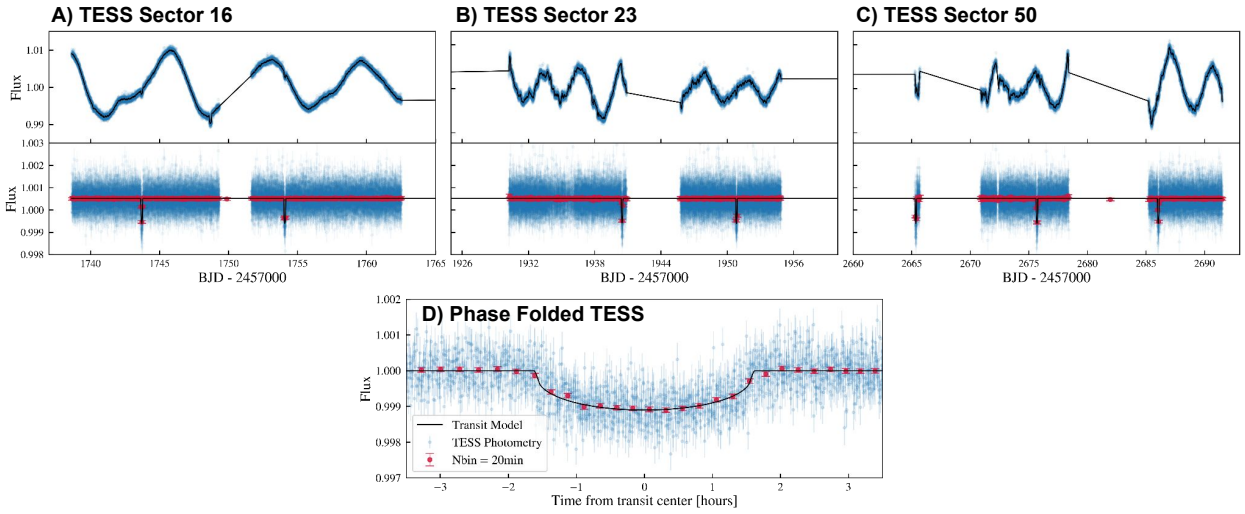

Figure 3.1 TESS lightcurves of TOI-2076 from A) Sector 16, B) Sector 23, and C) Sector 50. The top row shows the TESS photometry (blue points) with along with a transit model for TOI-2076 b + GP model (red) to account for stellar activity. The middle panel shows the photometry after subtracting the quasi-periodic GP model, revealing the TOI-2076 b transits. Panel D) shows the phase-folded TESS photometry phased to the orbital period of TOI-2076 b, with the transit model overlaid. Figure is from Frazier et al. (2023).

observations could constrain the eccentricity further.

3.3 Rossiter McLaughlin Effect

To model the RM effect, I used the `rmfit` package (see Stefánsson et al., 2022), which implements the RM effect model from Hirano et al. (2011b). Hirano et al. (2011b) takes into account stellar rotation, macroturbulence, and thermal, instrumental, and pressure broadening in the stellar absorption line profile to create a more accurate RM effect model. For the model, I placed informative priors on the transit parameters (P, T_C, $R_p/R_\star$, i, $a/R_\star$) as constrained by the photometric analysis in Section 3.2.I placed informative priors on the limb-darkening parameters u_1 and u_2. To arrive at a self-consistent constraint on the 3D obliquity ψ, in the RM model, I follow the RM parameterization discussed in Stefánsson et al. (2022), which parameterises the RM model in terms of the sky-projected obliquity λ, stellar inclination ($\cos i_\star$), stellar rotation period (P_{rot}), and stellar radius ($R_\star$) as variables in the MCMC sampling. The $v \sin i_\star$ is then estimated

as $v \sin i_\star = v\sqrt{1 - \cos^2 i_\star}$, where I estimate the equatorial velocity as $v_{\rm eq} = v = 2\pi R_\star / {P_{\rm rot}}^3$. I then estimate the obliquity using,

$$\cos(\psi) = \sin(i_\star)\cos(\lambda)\sin(i) + \cos(i_\star)\cos(i), \tag{3.1}$$

where i is the orbital inclination of the planet. For the final MCMC fit, I ran 100 walkers using the `emcee` package (Foreman-Mackey et al., 2013) for 30,000 steps after removing 2,000 steps as burn-in steps. To determine that the chains were converged, I leveraged a few methods. First, I verified that the Gelman-Rubin (GR) statistic was within $\ll$1% of unity. However, the GR statistic has limitations to assess convergence, especially when the walkers are not independent (see e.g., discussion in Hogg and Foreman-Mackey, 2018), so in addition to the GR statistic, I follow the suggestion in Hogg and Foreman-Mackey (2018) and estimated the autocorrelation length of our chains, where the mean autocorrelation length was $\tau_{\rm mean} = 202$, and the maximum autocorrelation length was $\tau_{\rm max} = 261$. From running 30,000 steps, this ensures that each chain has at least 100 independent samples, which is more than the chain length of 50τ as suggested in the `emcee` documentation[4]. From these lines of evidence combined with visual inspection of the chains suggesting convergence, I conclude the chains are well mixed.

To account for the RV trend seen during the observations, I simultaneously fit the RM effect with a RV slope. I also experimented with adding a quadratic curvature to the slope. However, doing so did not significantly improve the resulting fit where the difference in the Bayesian Information Criterion was $\Delta{\rm BIC} = 3.0$ in favor of the quadratic model, suggesting only a modest statistical preference for the more complicated model, where both models yielded the same constraints on the key parameters of interest of $v \sin i_\star$ and λ. Given the low statistical preference, I adopted the simpler linear model. As the semi-amplitude of the planet K—which is currently unconstrained as TOI-2076 b does not have a measured mass—is degenerate with the linear RV

[3]This broadly follows the methodology in Masuda and Winn (2020) to account for the fact that $v \sin i_\star$ and $v_{\rm eq}$ are not independent variables. As I am assuming solid body rotation, the equatorial velocity equals the rotational velocity of the star.

[4]See notes here: `https://emcee.readthedocs.io/en/latest/tutorials/autocorr/\#autocorr`

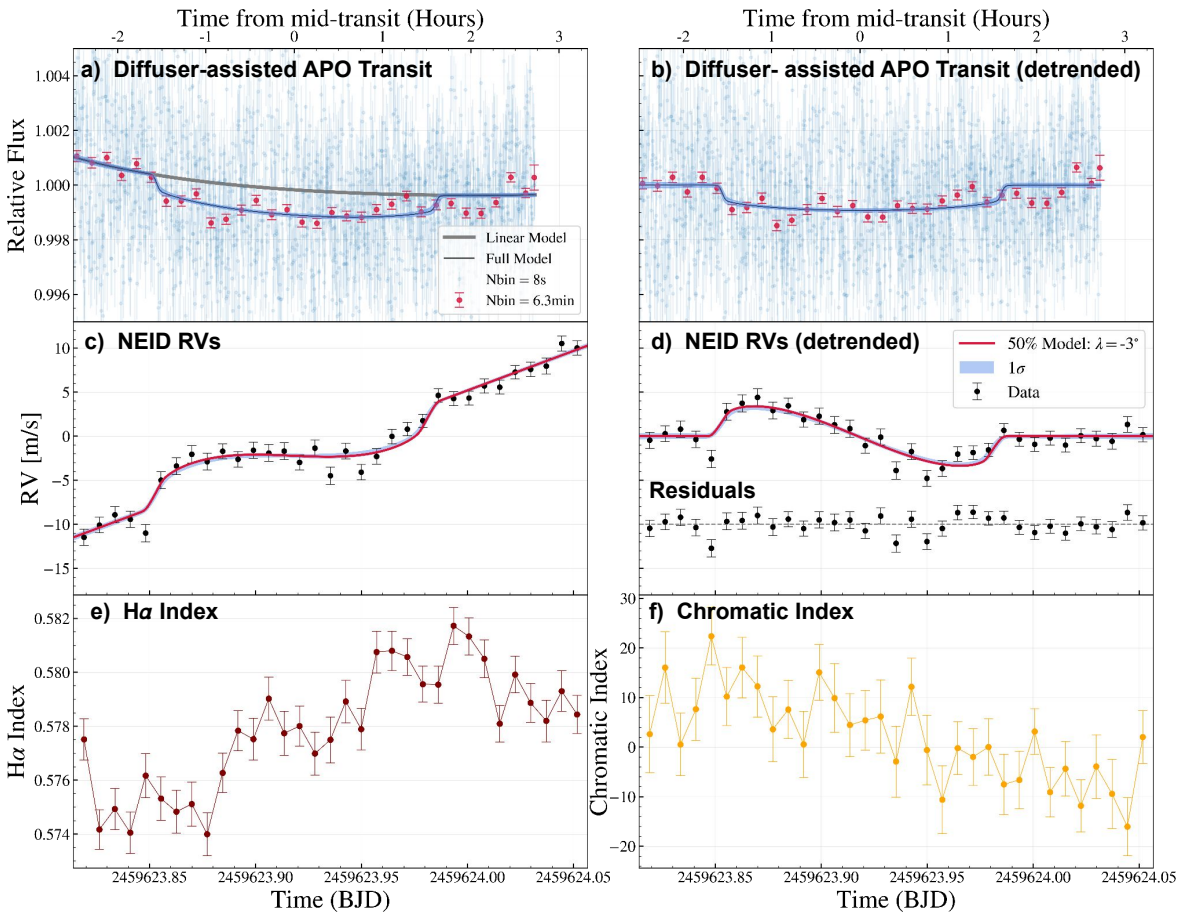

Figure 3.2 a) Diffuser-assisted photometry from APO with the transit model from the joint APO and TESS fit overlaid in blue. The linear model of the airmass is shown in grey. b) Diffuser-assisted photometry and the joint transit model detrended from the linear model of the airmass. c) NEID RV data during the transit of TOI-2076 b revealing a clear detection of the RM effect. I attribute the positive slope to stellar activity. d) NEID RV data detrended from the overall upward slope and the corresponding residuals. e) Hα index from NEID RV observations. f) Chromatic index (CRX) from NEID RV observations. The data are available as data-behind the figure. Figure is from Frazier et al. (2023).

slope during the short observing baseline, I elected to fix the semi-amplitude of the planet to zero and let the slope parameter fully account for the long-term RV trend during the observations. Table 3.3 summarizes the input priors and the best-fit posterior values.

Figure 3.2 shows a plot of the data along with the best-fit RM effect model. Our best fit model suggests a sky-projected velocity of $v \sin i = 5.27^{+0.24}_{-0.29}\,\mathrm{km/s}$, a sky-projected obliquity of $\lambda = -3^{+16}_{-15}{}^{\circ}$, and a obliquity of $\psi = 18^{+10}_{-9}{}^{\circ}$ ($\psi < 34^{\circ}$ at 95% confidence). The $v \sin i_{\star}$ value

Table 3.3 Summary of priors and resulting posteriors for the RM analysis. $\mathcal{N}(m, \sigma)$ denotes a normal prior with mean m, and standard deviation σ; $\mathcal{U}(a, b)$ denotes a uniform prior with a start value a and end value b.

Parameter	Description	Priors	Posteriors
MCMC Input Parameters:			
T_C ($\mathrm{BJD_{TDB}}$)	Transit midpoint	$\mathcal{N}(2458743.7247, 0.0025)$	2458743.7219 ± 0.0019
P	Orbital period (days)	$\mathcal{N}(10.35527, 0.00003)$	10.355235 ± 0.00002
R_p/R_*	Radius ratio	$\mathcal{N}(0.0284, 0.0011)$	0.02881 ± 0.00095
a/R_*	Scaled semi-major axis	$\mathcal{N}(24.87, 0.31)$	25.07 ± 0.28
i	Transit inclination (°)	$\mathcal{N}(89.72, 0.18)$	89.65 ± 0.17
e	Eccentricity	0.	0
ω	Argument of periastron (°)	90.	90.
K	RV semi-amplitude (m/s)	0	0
γ	NEID RV offset (m/s)	$\mathcal{U}(-50, 50)$	-0.59 ± 0.18
u_1	Linear limb darkening parameter	$\mathcal{N}(0.35, 0.1)$	$0.416_{\pm}0.098$
u_2	Quadratic limb darkening parameter	$\mathcal{N}(0.32, 0.1)$	0.332 ± 0.050
β	Intrinsic stellar line width (km/s)	$\mathcal{N}(6.0, 1.0)$	5.4 ± 1.0
λ	Sky-projected obliquity (deg)	$\mathcal{U}(-180, 180)$	-3^{+16}_{-15}
$R_\star$	Radius of star ($\mathrm{R_\odot}$)	$\mathcal{N}(0.772, 0.015)$	0.774 ± 0.015
P_{rot}	Stellar rotation period (days)	$\mathcal{N}(7.27, 0.23)$	7.21 ± 0.22
$\cos i_\star$	Cosine of stellar inclination	$\mathcal{U}(0, 1)$	$0.2^{+0.18}_{-0.14}$
$\dot{\gamma}$	Slope of Radial Velocities (m/s/day)	$\mathcal{U}(-500, 500)$	89.7 ± 2.4
Derived Parameters:			
$v \sin i_\star$	Projected rotational velocity (km/s)	-	$5.27^{+0.24}_{-0.22}$
$i_\star$	Stellar inclination (deg)	-	79^{+8}_{-11}
ψ	Obliquity (deg)	-	18^{+10}_{-9}

agrees with the $v \sin i_\star = 5 \pm 1\,\mathrm{km/s}$ from the spectral-broadening measurements in Table 3.1. The obliquity value of $\psi = 18^{+10}_{-9}\,^\circ$ suggests that TOI-2076 b is on a well-aligned orbit.

As an additional test, I fit the RM effect using the more conventional parameterization of λ and $v \sin i$ placing uniform priors on $v \sin i_\star$ from 0 to 10km/s, instead of the $\cos i_\star$, $R_\star$, and P_{rot} parameterization discussed above. In doing so, I obtain a λ of $-3^{+13}_{-14}\,^\circ$, and $v \sin i_\star = 5.28^{+0.23}_{-0.28}\,\mathrm{km/s}$, which agrees with the values above. I elect to use the former parameterization to arrive at a self-consistent constraint of the obliquity, ψ.

Chapter 4

Discussion

4.1 Impact of Stellar Activity on the RM analysis

TOI-2076 shows clears signatures of stellar activity due to its young age of ($204 \pm 50\,\mathrm{MYr}$). The TESS data shows photometric variations with an amplitude of $\sim$1% (Figure 3.1). Additionally, Figure 3.2 shows a clear trend in the RVs during the RM observations with an amplitude of $\sim$20 m/s across the full 5.5 hour observing baseline. This trend is in the opposite direction to what I would expect due to the planet-induced stellar radial velocity, which I estimated to have a RV semi-amplitude of $K = 2.0^{+1.5}_{-0.8}\,\mathrm{m/s}$ (assuming a predicted mass of $6.3^{+4.5}_{-2.6} M_{\oplus}$ using the mass-radius relation from the `Forecaster` package (Chen and Kipping, 2017)). Such inverse trends have been previously reported in RM observations of other young systems: Wirth et al. (2021) observed an RV trend of $\sim$75 m/s over a similar baseline ($\sim 19\,\mathrm{m/s/hr}$) in RM observations of the 60 Myr old TOI-942b, and Benatti et al. (2019) observed an even larger RV trend of $\sim$150 m/s ($\sim 25\,\mathrm{m/s/hr}$) for the 45 Myr old DS Tuc A b.

In addition to the photometry and the radial velocities, Figure 3.2 also shows the Hα index along with the chromatic index (CRX), both of which show slow trends during the RM observations. I calculated both indices following the definition in Zechmeister et al. (2018). The Hα index is particularly sensitive to flares (e.g., Ichimoto and Kurokawa, 1984), and the lack of flare-like features and/or high-frequency variations suggests that no large flares occurred during the observations, consistent with the photometric observations. The chromatic index, CRX, is defined in Zechmeister et al. (2018) as the best-fit straight line slope fitted to order-by-order RVs as a function of wavelength, it is measured in velocity per unit wavelength ratio. A non-zero CRX value signifies that a trend is seen in the order-by-order RVs as a function of wavelength, a strong indication of stellar activity. From the CRX values shown in Figure 3.2, I see indications of a chromaticity in the RVs. To further examine this behavior, I split the radial velocity data in two groups of 'blue' orders (3975–6447Å) and 'red' orders (6447–8920Å) as seen in Figure 4.1. Separate RV fits of these 'blue' and 'red' extractions resulted in RV slopes of $\dot{\gamma}_{\mathrm{blue}} = 91.3^{+2.4}_{-2.5}\,\mathrm{m/s/day}$, and $\dot{\gamma}_{\mathrm{red}} = 62.9 \pm 8.5\,\mathrm{m/s/day}$. The lower slope value seen in the red wavelengths is expected if the

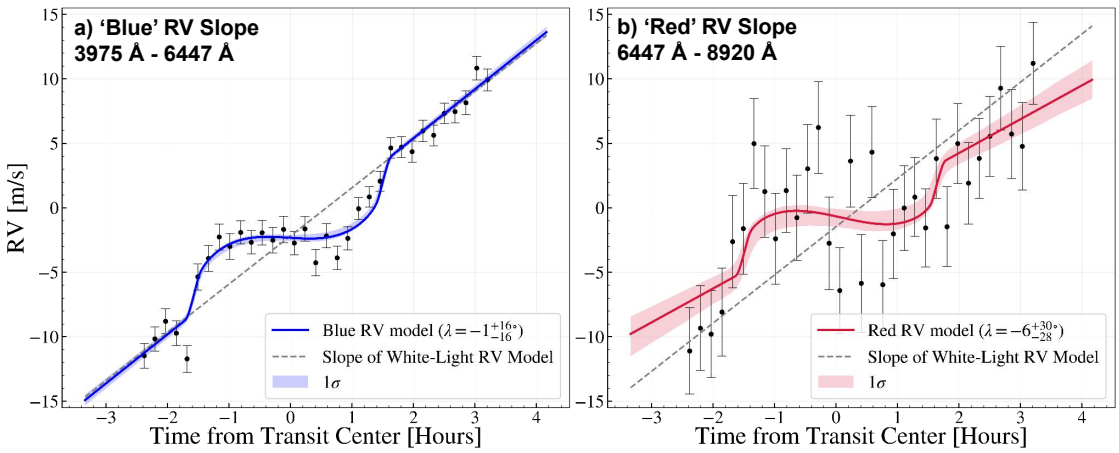

Figure 4.1 Comparing an RM fit to 'blue-only' RVs (a) and 'red-only' RVs (b). The RV curve for the 'blue-only' RV orders spans orders from 3975–6447 Å and the 'red-only' orders span orders from 6447–8920 Å. For comparison, the slope of the 'white-light' RV model used in the full analysis is overplotted as the grey-dashed line in both panels. The slope in the blue orders is steeper than in the red, suggesting the RV slope is due to stellar activity such as a spot on the surface of the star. Figure is from Frazier et al. (2023).

activity signature is due to a starspot with a differing contrast as a function of wavelength compared to the stellar photosphere, further confirming that the slope is due to activity. Best-fit RM models to the 'blue' and 'red' RV extractions returned $v \sin i$, λ and ψ values consistent with the values ('white-light') reported in Table 3.3, suggesting that our treatment of a simple line to remove the RV trend is sufficient to remove the activity signature and does not impact the determination of the obliquity.

To further estimate the expected RV impact of a possible starspot moving on the stellar surface during the RM observations, the `SOAP2.0` code (Dumusque et al., 2014) was used. For the starspot simulation, a stellar inclination of $i_\star = 80°$ was assumed, consistent with the median value from our RM analysis. Experimenting placing different spots of different sizes showed that placing two circular spots with a temperature contrast of $\Delta 500$ K of radius $0.23 R_\star$ (covering 2.6% of the visible hemisphere) at latitudes of 30 degrees, resulted in $\sim 1\%$ photometric variations peak-to-valley, consistent with the amplitude of variations seen in the TESS photometry. The expected peak-to-valley RV variations from such spots was $\sim$150 m/s, which would cause a $\sim$19 m/s RV variation during the 5.5 h observing baseline. This is in good agreement with the RV trend I see

in Figure 3.2c. I note that this is not a unique solution, as due to degeneracies between different spot parameters, including spot size, latitude, and contrast, there is a good possibility that different spot configurations could also explain the observed photometry. However, as a configuration exists that is compatible with the TESS photometry and the NEID radial velocities, I conclude that the observed RV slope is likely due to stellar activity.

4.2 Obliquities as a Function of Age

TOI-2076 b joins a small but growing group of planets in young systems with multiple transiting planets with measured obliquities. Figure 4.2 compares the obliquity of TOI-2076 b to obliquity measurements of other known exoplanets in single and multi transiting planet systems as a function of age of the system.

For systems with a single transiting planet, I see that highly misaligned planets are only seen for ages $\gtrsim$200 Myr, where the Kepler-63b system—hosting a Saturn-size planet in a 9.4 day orbit around a young 210MYr Sun-like star—is the youngest system hosting a highly misaligned planet with $\lambda = -135^{+21.2}_{-26.8}{}^{\circ}$, and $\psi = 114.6^{+16.6}_{-12.5}{}^{\circ}$ (Sanchis-Ojeda et al., 2013; Bourrier et al., 2023). For older systems ($\gtrsim$1 Gyr), there is a growing population of eccentric sub-Saturns that are on misaligned orbits, including WASP-107b (Rubenzahl et al., 2021), GJ 436 b (Bourrier et al., 2018, 2022), GJ 3470b (Stefánsson et al., 2022), HD 89345b (Bourrier et al., 2023), and HAT-P-11b (Hirano et al. (2011a) and Winn et al. (2010)). Three of these systems—WASP-107b, GJ 3470b, and HAT-P-11b—have known outer companions or candidate outer companions that have been suggested as possible paths to explain the misalignments of the inner transiting planets via gravitational interactions. However, the story is not fully clear, as the GJ 436b system does not have a known outer companion in the system, and there are some sub-Saturns on eccentric orbits that are observed to be on well-aligned orbits (e.g., K2-25b; Stefansson et al., 2020). This could possibly indicate that different formation mechanisms are at play. The fact that misaligned planets with high obliquities are only seen around systems with ages $\gtrsim$200 Myr, potentially points to

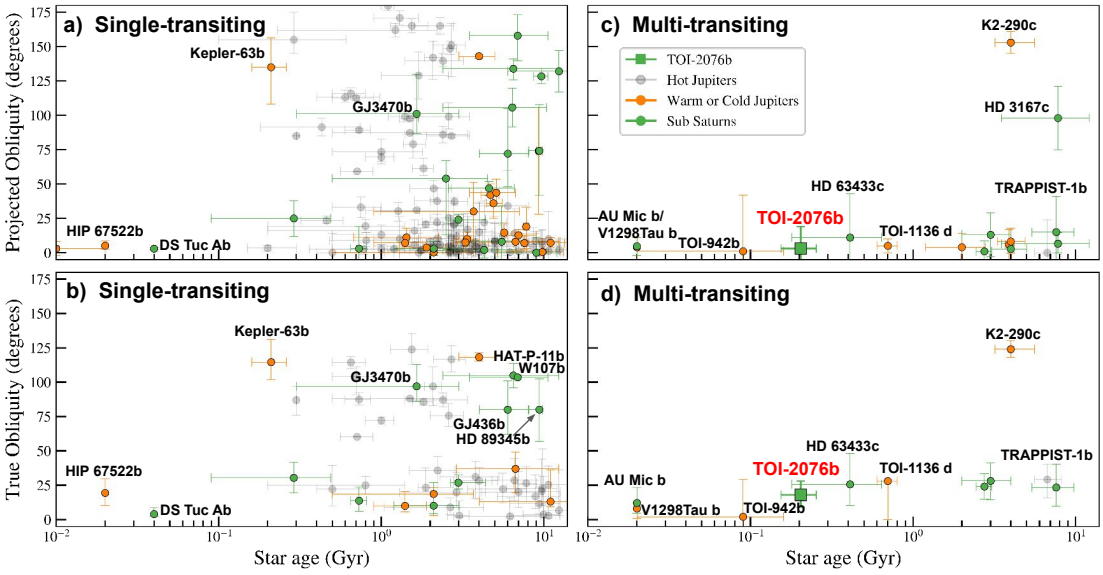

Figure 4.2 Sky-projected obliquities (a, c) and 3D obliquities (b, d) for planetary systems as a function of age for single-transiting (a, b), and multi-transiting (c, d) systems. Planets with masses $> 0.3\,\mathrm{M_J}$ and $a/R_\star < 10$ are classified hot Jupiters (black points), and as warm Jupiters if $a/R_\star > 10$ (orange points). Planets with masses $< 0.3\,\mathrm{M_J}$ are classified as sub-Saturns regardless of the value of $a/R_\star$. This classification system is adopted from Albrecht et al. (2022). Despite a lack of a mass measurement of TOI-2076 b I classify it as a sub-Saturn due to its radius and distance. The position of TOI-2076 b is highlighted in red. Obliquity measurements for systems excluding TOI-2076 are drawn from Albrecht et al. (2022), Dai et al. (2023), Bourrier et al. (2023), and the TEPCAT database (Southworth, 2011) where the error on the sky-projected obliquity was $\Delta\lambda < 40^\circ$, and the fractional error on the age of the system was less than 90%. W107b denotes WASP-107b. Figure is from Frazier et al. (2023).

that the origin of misalignment might not be primordial and is rather caused by dynamical interactions later on. However, the mechanisms that are often invoked to explain misalignments—secular resonance crossings due to a disappearing disk and a massive outer companion (Petrovich et al., 2020), and Von Zeipel-Kozai-Lidov oscillations (Fabrycky and Tremaine, 2007; Naoz, 2016)—occur on relatively fast timescales of $10^5 - 10^6$yrs, so the lack of misalignments of the youngest small planets continues to be noteworthy. Additional obliquity constraints of the very youngest systems (< 100MYr) will be particularly valuable.

For the systems with multiple transiting planets (multi-transiting systems), I see from Figure 4.2 that there are no known young multi-transiting systems with ages $\lesssim 1 - 3$ Gyr on misaligned orbits. I see that there are two older misaligned multi-transiting systems: K2-290 (Hjorth et al.,

2021), and HD 3167c (Dalal et al., 2019), with ages $\gtrsim$3 GYr. Interestingly, these systems have contrasting architectures: K2-290 hosts two planets, K2-290b and c in a co-planar orbit, whereas HD 3167b and c have a mutual inclinations of $\sim$90 degrees (Bourrier et al., 2021). To explain the misalignments, for the K2-290 system it has been suggested that an outer star K2-290 B (projected separation of 110 au) could have tilted the protoplanetary disk of K2-290 A, causing K2-290b and c to form coplanar in an initially misaligned disk (Hjorth et al., 2021). An alternative formation scenario was suggested by Best and Petrovich (2022), in which the third star in the triple system, K2-290 C (projected separation of 2500 au), could be responsible for the misalignment of both planets through gravitational perturbations at much longer timescales (typically $\gtrsim 100$ Myr). For the HD 3167 system, Bourrier et al. (2021) suggest the that the perpendicular architecture likely arose from the outer planet being tilted through gravitational interactions with a possible outer companion, while the inner ultra-short period planet likely retained a low obliquity due to tight tidal-coupling with the host star.

In contrast to the misaligned multi-planet systems, for TOI-2076 b there are multiple lines of evidence suggesting that TOI-2076 b formed via a more dynamically benign process of smooth disk migration in an initially well-aligned disk. First, the large $a/R_\star \sim 25$ value for TOI-2076 b makes tidal realignment inefficient, making TOI-2076 b a pristine probe of the initial formation angle. This, combined with the currently observed low-obliquity of TOI-2076 b, disfavors a scenario where TOI-2076 b experienced a high degree of misalignment that was subsequently realigned. Second, the planets in the TOI-2076 system orbit close to period commensurabilities (b and c at close to 2:1 resonance; c and d close to 5:3 resonance) with clear TTVs observed in the system (Osborn et al., 2022), which demonstrates that the planets in the TOI-2076 system are tightly gravitationally interacting. Therefore, an appealing formation scenario for the compact TOI-2076 b system is through smooth disk migration within an initially well-aligned protoplanetary disk (e.g., Goldreich and Tremaine, 1979, 1980), where the planets migrated into their resonant orbits that I see today. Future RM effect observations of TOI-2076 c and d will help constrain the coplanarity of the system, which through these lines of evidence I would expect to be likely well-aligned with

the orbit of planet b. TOI-2076b is similar to the recently studied TOI-1136 system (Dai et al., 2023), which is a compact network of at least 6 transiting planets in a resonant chain that likely formed through smooth disk migration in an initially well-aligned disk.

Chapter 5

Conclusion

Using high precision in-transit spectroscopic observations with the NEID spectrograph on the WIYN 3.5m Telescope at Kitt Peak Observatory, we determined that the young (204 ± 50 Myr) sub-Neptune planet TOI-2076 b has a low sky-projected obliquity of $\lambda = -3^{+16}_{-15}{}^{\circ}$. Leveraging knowledge of the size of the star, and the stellar rotation period, we estimate an obliquity of $\psi = 18^{+10}_{-9}{}^{\circ}$ and a stellar inclination of $i_{\star} = 79^{+8}_{-11}{}^{\circ}$ suggesting that TOI-2076 b is on an orbit well-aligned with the stellar equator of its host star. Three sectors of data from the TESS spacecraft along with precise diffuser-assisted photometry from ARCTIC on the ARC 3.5 m telescope at APO were used to precisely constrain the orbital parameters of the planet.

TOI-2076 b joins a small, but growing sample of young multi-planet systems on well-aligned orbits. It is the fourth planet with an age ≤ 300 Myr in a multi-transiting system with an obliquity measurement. The well-aligned orbit of TOI-2076 b together with the compact multi-planet configuration that shows evidence of transit timing variations suggests that the TOI-2076 system likely formed via convergent disk-migration in an initially well-aligned disk. This would suggest that TOI-2076c and d are likely coplanar to TOI-2076 b. Additional RM observations of the outer planets are needed to confirm this hypothesis.

In addition, due to its brightness, TOI-2076 hosts some of the most accessible young planets for atmospheric characterization. With a measurement of its obliquity, the architecture of the TOI-2076 system is now better understood, which will help place any future follow-up observations—such as atmospheric characterization—in further context.

Bibliography

Albrecht, S., Winn, J. N., Johnson, J. A., Howard, A. W., Marcy, G. W., Butler, R. P., Arriagada, P., Crane, J. D., Shectman, S. A., Thompson, I. B., Hirano, T., Bakos, G., and Hartman, J. D. (2012). Obliquities of Hot Jupiter Host Stars: Evidence for Tidal Interactions and Primordial Misalignments. *ApJ*, 757(1):18.

Albrecht, S. H., Dawson, R. I., and Winn, J. N. (2022). Stellar Obliquities in Exoplanetary Systems. *PASP*, 134(1038):082001.

Albrecht, S. H., Marcussen, M. L., Winn, J. N., Dawson, R. I., and Knudstrup, E. (2021). A Preponderance of Perpendicular Planets. *ApJL*, 916(1):L1.

Benatti, S., Nardiello, D., Malavolta, L., Desidera, S., Borsato, L., Nascimbeni, V., Damasso, M., D'Orazi, V., Mesa, D., Messina, S., Esposito, M., Bignamini, A., Claudi, R., Covino, E., Lovis, C., and Sabotta, S. (2019). A possibly inflated planet around the bright young star DS Tucanae A. *A&A*, 630:A81.

Benz, W., Broeg, C., Fortier, A., Rando, N., Beck, T., Beck, M., Queloz, D., Ehrenreich, D., Maxted, P. F. L., Isaak, K. G., Billot, N., Alibert, Y., Alonso, R., António, C., Asquier, J., Bandy, T., Bárczy, T., Barrado, D., Barros, S. C. C., Baumjohann, W., Bekkelien, A., Bergomi, M., Biondi, F., Bonfils, X., Borsato, L., Brandeker, A., Busch, M. D., Cabrera, J., Cessa, V., Charnoz, S., Chazelas, B., Collier Cameron, A., Corral Van Damme, C., Cortes, D., Davies, M. B., Deleuil, M., Deline, A., Delrez, L., Demangeon, O., Demory, B. O., Erikson, A., Farinato, J., Fossati, L., Fridlund, M., Futyan, D., Gandolfi, D., Garcia Munoz, A., Gillon, M., Guterman, P., Gutierrez, A., Hasiba, J., Heng, K., Hernandez, E., Hoyer, S., Kiss, L. L., Kovacs, Z., Kuntzer, T., Laskar, J., Lecavelier des Etangs, A., Lendl, M., López, A., Lora, I., Lovis, C., Lüftinger, T., Magrin, D., Malvasio, L., Marafatto, L., Michaelis, H., de Miguel, D., Modrego, D., Munari, M., Nascimbeni, V., Olofsson, G., Ottacher, H., Ottensamer, R., Pagano, I., Palacios, R., Pallé, E., Peter, G., Piazza, D., Piotto, G., Pizarro, A., Pollaco, D., Ragazzoni, R., Ratti, F., Rauer, H., Ribas, I., Rieder, M., Rohlfs, R., Safa, F., Salatti, M., Santos, N. C., Scandariato, G., Ségransan, D., Simon, A. E., Smith, A. M. S., Sordet, M., Sousa, S. G., Steller, M., Szabó, G. M., Szoke, J., Thomas, N., Tschentscher, M., Udry, S., Van Grootel, V., Viotto, V., Walter, I., Walton, N. A., Wildi, F., and Wolter, D. (2021). The CHEOPS mission. *Experimental Astronomy*, 51(1):109–151.

Best, S. and Petrovich, C. (2022). The Chaotic History of the Retrograde Multi-planet System in K2-290A Driven by Distant Stars. *ApJL*, 925(1):L5.

Bourrier, Lovis, C., Cretignier, M., Allart, R., Dumusque, X., Delisle, J.-B., Deline, A., Sousa, S. G., Adibekyan, V., Alibert, Y., Barros, S. C. C., Borsa, F., Cristiani, S., Demangeon, O., Ehrenreich, D., Figueira, P., González Hernández, J. I., Lendl, M., Lillo-Box, J., Lo Curto, G., Di Marcantonio, P., Martins, C. J. A. P., Mégevand, D., Mehner, A., Micela, G., Molaro, P., Oshagh, M., Palle, E., Pepe, F., Poretti, E., Rebolo, R., Santos, N. C., Scandariato, G., Seidel, J. V., Sozzetti, A., Suárez Mascareño, A., and Zapatero Osorio, M. R. (2021). The rossiter-mclaughlin effect revolutions: an ultra-short period planet and a warm mini-neptune on perpendicular orbits. *A&A*, 654:A152.

Bourrier, V., Attia, O., Mallonn, M., Marret, A., Lendl, M., Konig, P. C., Krenn, A., Cretignier, M., Allart, R., Henry, G., Bryant, E., Leleu, A., Nielsen, L., Hebrard, G., Hara, N., Ehrenreich, D., Seidel, J., dos Santos, L., Lovis, C., Bayliss, D., Cegla, H. M., Dumusque, X., Boisse, I., Boucher, A., Bouchy, F., Pepe, F., Lavie, B., Rey Cerda, J., Ségransan, D., Udry, S., and Vrignaud, T. (2023). DREAM. I. Orbital architecture orrery. *A&A*, 669:A63.

Bourrier, V., Lovis, C., Beust, H., Ehrenreich, D., Henry, G. W., Astudillo-Defru, N., Allart, R., Bonfils, X., Ségransan, D., Delfosse, X., Cegla, H. M., Wyttenbach, A., Heng, K., Lavie, B., and Pepe, F. (2018). Orbital misalignment of the Neptune-mass exoplanet GJ 436b with the spin of its cool star. *Nature*, 553:477–480.

Bourrier, V., Zapatero Osorio, M. R., Allart, R., Attia, O., Cretignier, M., Dumusque, X., Lovis, C., Adibekyan, V., Borsa, F., Figueira, P., González Hernández, J. I., Mehner, A., Santos, N. C., Schmidt, T., Seidel, J. V., Sozzetti, A., Alibert, Y., Casasayas-Barris, N., Ehrenreich, D., Lo Curto, G., Martins, C. J. A. P., Di Marcantonio, P., Mégevand, D., Nunes, N. J., Palle, E., Poretti, E., and Sousa, S. G. (2022). The polar orbit of the warm Neptune GJ 436b seen with VLT/ESPRESSO. *A&A*, 663:A160.

Center, T. O. (2022). Tess planet count and papers.

Chen, J. and Kipping, D. (2017). Probabilistic Forecasting of the Masses and Radii of Other Worlds. *ApJ*, 834:17.

Clough, S. A., Shephard, M. W., Mlawer, E. J., Delamere, J. S., Iacono, M. J., Cady-Pereira, K., Boukabara, S., and Brown, P. D. (2005). Atmospheric radiative transfer modeling: a summary of the AER codes. *JQSRT*, 91:233–244.

Coelho, P., Barbuy, B., Meléndez, J., Schiavon, R. P., and Castilho, B. V. (2005). A library of high resolution synthetic stellar spectra from 300 nm to 1.8 μm with solar and α-enhanced composition. *A&A*, 443(2):735–746.

Collins, K. A., Kielkopf, J. F., Stassun, K. G., and Hessman, F. V. (2017). AstroImageJ: Image Processing and Photometric Extraction for Ultra-precise Astronomical Light Curves. *AJ*, 153(2):77.

Cosentino, R., Lovis, C., Pepe, F., Cameron, A. C., Latham, D. W., Molinari, E., Udry, S., Bezawada, N., Black, M., Born, A., Buchschacher, N., Charbonneau, D., Figueira, P., Fleury, M., Galli, A., Gallie, A., Gao, X., Ghedina, A., Gonzalez, C., Gonzalez, M., Guerra, J., Henry, D.,

Horne, K., Hughes, I., Kelly, D., Lodi, M., Lunney, D., Maire, C., Mayor, M., Micela, G., Ordway, M. P., Peacock, J., Phillips, D., Piotto, G., Pollacco, D., Queloz, D., Rice, K., Riverol, C., Riverol, L., Juan, J. S., Sasselov, D., Segransan, D., Sozzetti, A., Sosnowska, D., Stobie, B., Szentgyorgyi, A., Vick, A., and Weber, L. (2012). Harps-N: the new planet hunter at TNG. 8446:84461V.

Crass, J., Gaudi, B. S., Leifer, S., Beichman, C., Bender, C., Blackwood, G., Burt, J. A., Callas, J. L., Cegla, H. M., Diddams, S. A., Dumusque, X., Eastman, J. D., Ford, E. B., Fulton, B., Gibson, R., Halverson, S., Haywood, R. D., Hearty, F., Howard, A. W., Latham, D. W., Löhner-Böttcher, J., Mamajek, E. E., Mortier, A., Newman, P., Plavchan, P., Quirrenbach, A., Reiners, A., Robertson, P., Roy, A., Schwab, C., Seifahrt, A., Szentgyorgyi, A., Terrien, R., Teske, J. K., Thompson, S., and Vasisht, G. (2021). Extreme precision radial velocity working group final report.

Dai, F., Masuda, K., Beard, C., Robertson, P., Goldberg, M., Batygin, K., Bouma, L., Lissauer, J. J., Knudstrup, E., Albrecht, S., Howard, A. W., Knutson, H. A., Petigura, E. A., Weiss, L. M., Isaacson, H., Kristiansen, M. H., Osborn, H., Wang, S., Wang, X.-Y., Behmard, A., Greklek-McKeon, M., Vissapragada, S., Batalha, N. M., Brinkman, C. L., Chontos, A., Crossfield, I., Dressing, C., Fetherolf, T., Fulton, B., Hill, M. L., Huber, D., Kane, S. R., Lubin, J., MacDougall, M., Mayo, A., Močnik, T., Akana Murphy, J. M., Rubenzahl, R. A., Scarsdale, N., Tyler, D., Zandt, J. V., Polanski, A. S., Schwengeler, H. M., Terentev, I. A., Benni, P., Bieryla, A., Ciardi, D., Falk, B., Furlan, E., Girardin, E., Guerra, P., Hesse, K. M., Howell, S. B., Lillo-Box, J., Matthews, E. C., Twicken, J. D., Villaseñor, J., Latham, D. W., Jenkins, J. M., Ricker, G. R., Seager, S., Vanderspek, R., and Winn, J. N. (2023). TOI-1136 is a Young, Coplanar, Aligned Planetary System in a Pristine Resonant Chain. *AJ*, 165(2):33.

Dalal, S., Hébrard, G., Lecavelier des Étangs, A., Petit, A. C., Bourrier, V., Laskar, J., König, P. C., and Correia, A. C. M. (2019). Nearly polar orbit of the sub-Neptune HD 3167 c. Constraints on the dynamical history of a multi-planet system. *A&A*, 631:A28.

Dumusque, X., Boisse, I., and Santos, N. C. (2014). SOAP 2.0: A Tool to Estimate the Photometric and Radial Velocity Variations Induced by Stellar Spots and Plages. *ApJ*, 796:132.

Eastman, J. D., Rodriguez, J. E., Agol, E., Stassun, K. G., Beatty, T. G., Vanderburg, A., Gaudi, B. S., Collins, K. A., and Luger, R. (2019). EXOFASTv2: A public, generalized, publication-quality exoplanet modeling code. *arXiv e-prints (submitted to PASP)*.

Espinoza, N., Kossakowski, D., and Brahm, R. (2019). juliet: a versatile modelling tool for transiting and non-transiting exoplanetary systems. *MNRAS*, 490(2):2262–2283.

Fabrycky, D. and Tremaine, S. (2007). Shrinking Binary and Planetary Orbits by Kozai Cycles with Tidal Friction. *ApJ*, 669(2):1298–1315.

Foreman-Mackey, D., Agol, E., Ambikasaran, S., and Angus, R. (2017). Fast and Scalable Gaussian Process Modeling with Applications to Astronomical Time Series. *AJ*, 154(6):220.

Foreman-Mackey, D., Hogg, D. W., Lang, D., and Goodman, J. (2013). emcee: The mcmc hammer. *PASP*, 125:306–312.

Frazier, R. C., Stefá nsson, G., Mahadevan, S., Yee, S. W., Cañas, C. I., Winn, J. N., Luhn, J., Dai, F., Doyle, L., Cegla, H., Kanodia, S., Robertson, P., Wisniewski, J., Bender, C. F., Dong, J., Gupta, A. F., Halverson, S., Hawley, S., Hebb, L., Holcomb, R., Kowalski, A., Libby-Roberts, J., Lin, A. S. J., McElwain, M. W., Ninan, J. P., Petrovich, C., Roy, A., Schwab, C., Terrien, R. C., and Wright, J. T. (2023). NEID reveals that the young warm neptune TOI-2076 b has a low obliquity. *The Astrophysical Journal Letters*, 944(2):L41.

Gaia Collaboration, Brown, A. G. A., Vallenari, A., Prusti, T., de Bruijne, J. H. J., Babusiaux, C., Biermann, M., Creevey, O. L., Evans, D. W., Eyer, L., Hutton, A., Jansen, F., Jordi, C., Klioner, S. A., Lammers, U., Lindegren, L., Luri, X., Mignard, F., Panem, C., Pourbaix, D., Randich, S., Sartoretti, P., Soubiran, C., Walton, N. A., Arenou, F., Bailer-Jones, C. A. L., Bastian, U., Cropper, M., Drimmel, R., Katz, D., Lattanzi, M. G., van Leeuwen, F., Bakker, J., Cacciari, C., Castañeda, J., De Angeli, F., Ducourant, C., Fabricius, C., Fouesneau, M., Frémat, Y., Guerra, R., Guerrier, A., Guiraud, J., Jean-Antoine Piccolo, A., Masana, E., Messineo, R., Mowlavi, N., Nicolas, C., Nienartowicz, K., Pailler, F., Panuzzo, P., Riclet, F., Roux, W., Seabroke, G. M., Sordo, R., Tanga, P., Thévenin, F., Gracia-Abril, G., Portell, J., Teyssier, D., Altmann, M., Andrae, R., Bellas-Velidis, I., Benson, K., Berthier, J., Blomme, R., Brugaletta, E., Burgess, P. W., Busso, G., Carry, B., Cellino, A., Cheek, N., Clementini, G., Damerdji, Y., Davidson, M., Delchambre, L., Dell'Oro, A., Fernández-Hernández, J., Galluccio, L., García-Lario, P., Garcia-Reinaldos, M., González-Núñez, J., Gosset, E., Haigron, R., Halbwachs, J. L., Hambly, N. C., Harrison, D. L., Hatzidimitriou, D., Heiter, U., Hernández, J., Hestroffer, D., Hodgkin, S. T., Holl, B., Janßen, K., Jevardat de Fombelle, G., Jordan, S., Krone-Martins, A., Lanzafame, A. C., Löffler, W., Lorca, A., Manteiga, M., Marchal, O., Marrese, P. M., Moitinho, A., Mora, A., Muinonen, K., Osborne, P., Pancino, E., Pauwels, T., Petit, J. M., Recio-Blanco, A., Richards, P. J., Riello, M., Rimoldini, L., Robin, A. C., Roegiers, T., Rybizki, J., Sarro, L. M., Siopis, C., Smith, M., Sozzetti, A., Ulla, A., Utrilla, E., van Leeuwen, M., van Reeven, W., Abbas, U., Abreu Aramburu, A., Accart, S., Aerts, C., Aguado, J. J., Ajaj, M., Altavilla, G., Álvarez, M. A., Álvarez Cid-Fuentes, J., Alves, J., Anderson, R. I., Anglada Varela, E., Antoja, T., Audard, M., Baines, D., Baker, S. G., Balaguer-Núñez, L., Balbinot, E., Balog, Z., Barache, C., Barbato, D., Barros, M., Barstow, M. A., Bartolomé, S., Bassilana, J. L., Bauchet, N., Baudesson-Stella, A., Becciani, U., Bellazzini, M., Bernet, M., Bertone, S., Bianchi, L., Blanco-Cuaresma, S., Boch, T., Bombrun, A., Bossini, D., Bouquillon, S., Bragaglia, A., Bramante, L., Breedt, E., Bressan, A., Brouillet, N., Bucciarelli, B., Burlacu, A., Busonero, D., Butkevich, A. G., Buzzi, R., Caffau, E., Cancelliere, R., Cánovas, H., Cantat-Gaudin, T., Carballo, R., Carlucci, T., Carnerero, M. I., Carrasco, J. M., Casamiquela, L., Castellani, M., Castro-Ginard, A., Castro Sampol, P., Chaoul, L., Charlot, P., Chemin, L., Chiavassa, A., Cioni, M. R. L., Comoretto, G., Cooper, W. J., Cornez, T., Cowell, S., Crifo, F., Crosta, M., Crowley, C., Dafonte, C., Dapergolas, A., David, M., David, P., de Laverny, P., De Luise, F., De March, R., De Ridder, J., de Souza, R., de Teodoro, P., de Torres, A., del Peloso, E. F., del Pozo, E., Delbo, M., Delgado, A., Delgado, H. E., Delisle, J. B., Di Matteo, P., Diakite, S., Diener, C., Distefano, E., Dolding, C., Eappachen, D., Edvardsson, B., Enke, H., Esquej, P., Fabre, C., Fabrizio, M., Faigler, S., Fedorets, G., Fernique, P., Fienga, A., Figueras, F., Fouron, C., Fragkoudi, F., Fraile, E., Franke, F., Gai, M., Garabato, D., Garcia-Gutierrez, A., García-Torres, M., Garofalo, A., Gavras, P., Gerlach, E., Geyer, R., Giacobbe, P., Gilmore, G., Girona, S., Giuffrida, G., Gomel, R., Gomez, A., Gonzalez-Santamaria, I., González-Vidal, J. J., Granvik, M., Gutiérrez-Sánchez, R., Guy,

L. P., Hauser, M., Haywood, M., Helmi, A., Hidalgo, S. L., Hilger, T., Hładczuk, N., Hobbs, D., Holland, G., Huckle, H. E., Jasniewicz, G., Jonker, P. G., Juaristi Campillo, J., Julbe, F., Karbevska, L., Kervella, P., Khanna, S., Kochoska, A., Kontizas, M., Kordopatis, G., Korn, A. J., Kostrzewa-Rutkowska, Z., Kruszyńska, K., Lambert, S., Lanza, A. F., Lasne, Y., Le Campion, J. F., Le Fustec, Y., Lebreton, Y., Lebzelter, T., Leccia, S., Leclerc, N., Lecoeur-Taibi, I., Liao, S., Licata, E., Lindstrøm, E. P., Lister, T. A., Livanou, E., Lobel, A., Madrero Pardo, P., Managau, S., Mann, R. G., Marchant, J. M., Marconi, M., Marcos Santos, M. M. S., Marinoni, S., Marocco, F., Marshall, D. J., Martin Polo, L., Martín-Fleitas, J. M., Masip, A., Massari, D., Mastrobuono-Battisti, A., Mazeh, T., McMillan, P. J., Messina, S., Michalik, D., Millar, N. R., Mints, A., Molina, D., Molinaro, R., Molnár, L., Montegriffo, P., Mor, R., Morbidelli, R., Morel, T., Morris, D., Mulone, A. F., Munoz, D., Muraveva, T., Murphy, C. P., Musella, I., Noval, L., Ordénovic, C., Orrù, G., Osinde, J., Pagani, C., Pagano, I., Palaversa, L., Palicio, P. A., Panahi, A., Pawlak, M., Peñalosa Esteller, X., Penttilä, A., Piersimoni, A. M., Pineau, F. X., Plachy, E., Plum, G., Poggio, E., Poretti, E., Poujoulet, E., Prša, A., Pulone, L., Racero, E., Ragaini, S., Rainer, M., Raiteri, C. M., Rambaux, N., Ramos, P., Ramos-Lerate, M., Re Fiorentin, P., Regibo, S., Reylé, C., Ripepi, V., Riva, A., Rixon, G., Robichon, N., Robin, C., Roelens, M., Rohrbasser, L., Romero-Gómez, M., Rowell, N., Royer, F., Rybicki, K. A., Sadowski, G., Sagristà Sellés, A., Sahlmann, J., Salgado, J., Salguero, E., Samaras, N., Sanchez Gimenez, V., Sanna, N., Santoveña, R., Sarasso, M., Schultheis, M., Sciacca, E., Segol, M., Segovia, J. C., Ségransan, D., Semeux, D., Shahaf, S., Siddiqui, H. I., Siebert, A., Siltala, L., Slezak, E., Smart, R. L., Solano, E., Solitro, F., Souami, D., Souchay, J., Spagna, A., Spoto, F., Steele, I. A., Steidelmüller, H., Stephenson, C. A., Süveges, M., Szabados, L., Szegedi-Elek, E., Taris, F., Tauran, G., Taylor, M. B., Teixeira, R., Thuillot, W., Tonello, N., Torra, F., Torra, J., Turon, C., Unger, N., Vaillant, M., van Dillen, E., Vanel, O., Vecchiato, A., Viala, Y., Vicente, D., Voutsinas, S., Weiler, M., Wevers, T., Wyrzykowski, Ł., Yoldas, A., Yvard, P., Zhao, H., Zorec, J., Zucker, S., Zurbach, C., and Zwitter, T. (2021). Gaia Early Data Release 3. Summary of the contents and survey properties. *A&A*, 649:A1.

Gaidos, E., Hirano, T., Lee, R. A., Harakawa, H., Hodapp, K., Jacobson, S., Kotani, T., Kudo, T., Kurokawa, T., Kuzuhara, M., Nishikawa, J., Omiya, M., Serizawa, T., Tamura, M., Ueda, A., and Vievard, S. (2023). Planet(esimal)s around stars with TESS (PAST) III: A search for triplet He I in the atmospheres of two 200 Myr-old planets. *MNRAS*, 518(3):3777–3783.

Gaudi, B. S., Seager, S., Mennesson, B., Kiessling, A., Warfield, K., Cahoy, K., Clarke, J. T., Domagal-Goldman, S., Feinberg, L., Guyon, O., Kasdin, J., Mawet, D., Plavchan, P., Robinson, T., Rogers, L., Scowen, P., Somerville, R., Stapelfeldt, K., Stark, C., Stern, D., Turnbull, M., Amini, R., Kuan, G., Martin, S., Morgan, R., Redding, D., Stahl, H. P., Webb, R., Alvarez-Salazar, O., Arnold, W. L., Arya, M., Balasubramanian, B., Baysinger, M., Bell, R., Below, C., Benson, J., Blais, L., Booth, J., Bourgeois, R., Bradford, C., Brewer, A., Brooks, T., Cady, E., Caldwell, M., Calvet, R., Carr, S., Chan, D., Cormarkovic, V., Coste, K., Cox, C., Danner, R., Davis, J., Dewell, L., Dorsett, L., Dunn, D., East, M., Effinger, M., Eng, R., Freebury, G., Garcia, J., Gaskin, J., Greene, S., Hennessy, J., Hilgemann, E., Hood, B., Holota, W., Howe, S., Huang, P., Hull, T., Hunt, R., Hurd, K., Johnson, S., Kissil, A., Knight, B., Kolenz, D., Kraus, O., Krist, J., Li, M., Lisman, D., Mandic, M., Mann, J., Marchen, L., Marrese-Reading, C., McCready, J., McGown, J., Missun, J., Miyaguchi, A., Moore, B., Nemati, B., Nikzad, S., Nissen, J., Novicki,

M., Perrine, T., Pineda, C., Polanco, O., Putnam, D., Qureshi, A., Richards, M., Riggs, A. J. E., Rodgers, M., Rud, M., Saini, N., Scalisi, D., Scharf, D., Schulz, K., Serabyn, G., Sigrist, N., Sikkia, G., Singleton, A., Shaklan, S., Smith, S., Southerd, B., Stahl, M., Steeves, J., Sturges, B., Sullivan, C., Tang, H., Taras, N., Tesch, J., Therrell, M., Tseng, H., Valente, M., Buren, D. V., Villalvazo, J., Warwick, S., Webb, D., Westerhoff, T., Wofford, R., Wu, G., Woo, J., Wood, M., Ziemer, J., Arney, G., Anderson, J., Maíz-Apellániz, J., Bartlett, J., Belikov, R., Bendek, E., Cenko, B., Douglas, E., Dulz, S., Evans, C., Faramaz, V., Feng, Y. K., Ferguson, H., Follette, K., Ford, S., García, M., Geha, M., Gelino, D., Götberg, Y., Hildebrandt, S., Hu, R., Jahnke, K., Kennedy, G., Kreidberg, L., Isella, A., Lopez, E., Marchis, F., Macri, L., Marley, M., Matzko, W., Mazoyer, J., McCandliss, S., Meshkat, T., Mordasini, C., Morris, P., Nielsen, E., Newman, P., Petigura, E., Postman, M., Reines, A., Roberge, A., Roederer, I., Ruane, G., Schwieterman, E., Sirbu, D., Spalding, C., Teplitz, H., Tumlinson, J., Turner, N., Werk, J., Wofford, A., Wyatt, M., Young, A., and Zellem, R. (2020). The habitable exoplanet observatory (habex) mission concept study final report.

Gaudi, B. S. and Winn, J. N. (2007). Prospects for the Characterization and Confirmation of Transiting Exoplanets via the Rossiter-McLaughlin Effect. *ApJ*, 655:550–563.

Goldreich, P. and Tremaine, S. (1979). The excitation of density waves at the Lindblad and corotation resonances by an external potential. *ApJ*, 233:857–871.

Goldreich, P. and Tremaine, S. (1980). Disk-satellite interactions. *ApJ*, 241:425–441.

Gullikson, K., Dodson-Robinson, S., and Kraus, A. (2014). Correcting for Telluric Absorption: Methods, Case Studies, and Release of the TelFit Code. *AJ*, 148:53.

Gupta, A. and Schlichting, H. E. (2019). Sculpting the valley in the radius distribution of small exoplanets as a by-product of planet formation: the core-powered mass-loss mechanism. *MNRAS*, 487(1):24–33.

Halverson, S., Terrien, R., Mahadevan, S., Roy, A., Bender, C., Stefánsson, G. K., Monson, A., Levi, E., Hearty, F., Blake, C., McElwain, M., Schwab, C., Ramsey, L., Wright, J., Wang, S., Gong, Q., and Roberston, P. (2016). A comprehensive radial velocity error budget for next generation Doppler spectrometers. In *Ground-based and Airborne Instrumentation for Astronomy VI*, volume 9908 of *Proc. SPIE*, page 99086P.

Hedges, C., Hughes, A., Zhou, G., David, T. J., Becker, J., Giacalone, S., Vanderburg, A., Rodriguez, J. E., Bieryla, A., Wirth, C., Atherton, S., Fetherolf, T., Collins, K. A., Price-Whelan, A. M., Bedell, M., Quinn, S. N., Gan, T., Ricker, G. R., Latham, D. W., Vanderspek, R. K., Seager, S., Winn, J. N., Jenkins, J. M., Kielkopf, J. F., Schwarz, R. P., Dressing, C. D., Gonzales, E. J., Crossfield, I. J. M., Matthews, E. C., Jensen, E. L. N., Furlan, E., Gnilka, C. L., Howell, S. B., Lester, K. V., Scott, N. J., Feliz, D. L., Lund, M. B., Siverd, R. J., Stevens, D. J., Narita, N., Fukui, A., Murgas, F., Palle, E., Sutton, P. J., Stassun, K. G., Bouma, L. G., Vezie, M., Villaseñor, J. N., Quintana, E. V., and Smith, J. C. (2021). TOI-2076 and TOI-1807: Two Young, Comoving Planetary Systems within 50 pc Identified by TESS that are Ideal Candidates for Further Follow Up. *AJ*, 162(2):54.

Hirano, T., Narita, N., Shporer, A., Sato, B., Aoki, W., and Tamura, M. (2011a). A Possible Tilted Orbit of the Super-Neptune HAT-P-11b. *PASJ*, 63:531.

Hirano, T., Suto, Y., Winn, J. N., Taruya, A., Narita, N., Albrecht, S., and Sato, B. (2011b). Improved Modeling of the Rossiter-McLaughlin Effect for Transiting Exoplanets. *ApJ*, 742:69.

Hjorth, M., Albrecht, S., Hirano, T., Winn, J. N., Dawson, R. I., Zanazzi, J. J., Knudstrup, E., and Sato, B. (2021). A backward-spinning star with two coplanar planets. *Proceedings of the National Academy of Science*, 118(8):e2017418118.

Hogg, D. W. and Foreman-Mackey, D. (2018). Data Analysis Recipes: Using Markov Chain Monte Carlo. *ApJS*, 236(1):11.

Holcomb, R. J., Robertson, P., Hartigan, P., Oelkers, R. J., and Robinson, C. (2022). SpinSpotter : An Automated Algorithm for Identifying Stellar Rotation Periods with Autocorrelation Analysis. *ApJ*, 936(2):138.

Huehnerhoff, J., Ketzeback, W., Bradley, A., Dembicky, J., Doughty, C., Hawley, S., Johnson, C., Klaene, M., Leon, E., McMillan, R., Owen, R., Sayres, C., Sheen, T., and Shugart, A. (2016). Astrophysical Research Consortium Telescope Imaging Camera (ARCTIC) facility optical imager for the Apache Point Observatory 3.5m telescope. volume 9908 of *Proc. SPIE*, page 99085H.

Ichimoto, K. and Kurokawa, H. (1984). Hα Red Asymmetry of Solar Flares. *SoPh*, 93(1):105–121.

Jenkins, J. M., Twicken, J. D., McCauliff, S., Campbell, J., Sanderfer, D., Lung, D., Mansouri-Samani, M., Girouard, F., Tenenbaum, P., Klaus, T., Smith, J. C., Caldwell, D. A., Chacon, A. D., Henze, C., Heiges, C., Latham, D. W., Morgan, E., Swade, D., Rinehart, S., and Vanderspek, R. (2016). The TESS science processing operations center. volume 9913 of *Proc. SPIE*, page 99133E.

Jurgenson, C., Fischer, D., McCracken, T., Sawyer, D., Szymkowiak, A., Davis, A., Muller, G., and Santoro, F. (2016). EXPRES: a next generation RV spectrograph in the search for earth-like worlds. 9908:99086T.

Kanodia, S. and Wright, J. (2018). Python Leap Second Management and Implementation of Precise Barycentric Correction (barycorrpy). *RNAAS*, 2:4.

Kipping, D. M. (2013). Efficient, uninformative sampling of limb darkening coefficients for two-parameter laws. *MNRAS*, 435:2152–2160.

Kreidberg, L. (2015). batman: BAsic Transit Model cAlculatioN in Python. *PASP*, 127:1161.

Lightkurve Collaboration, Cardoso, J. V. d. M., Hedges, C., Gully-Santiago, M., Saunders, N., Cody, A. M., Barclay, T., Hall, O., Sagear, S., Turtelboom, E., Zhang, J., Tzanidakis, A., Mighell, K., Coughlin, J., Bell, K., Berta-Thompson, Z., Williams, P., Dotson, J., and Barentsen, G. (2018). Lightkurve: Kepler and TESS time series analysis in Python. ASCL.

Masuda, K. and Winn, J. N. (2020). On the Inference of a Star's Inclination Angle from its Rotation Velocity and Projected Rotation Velocity. *AJ*, 159(3):81.

McCully, C., Crawford, S., Kovacs, G., Tollerud, E., Betts, E., Bradley, L., Craig, M., Turner, J., Streicher, O., Sipocz, B., Robitaille, T., and Deil, C. (2018). astropy/astroscrappy: v1.0.5 zenodo release.

McLaughlin, D. B. (1924). Some results of a spectrographic study of the Algol system. *ApJ*, 60.

Naoz, S. (2016). The Eccentric Kozai-Lidov Effect and Its Applications. *ARA&A*, 54:441–489.

Osborn, H. P., Bonfanti, A., Gandolfi, D., Hedges, C., Leleu, A., Fortier, A., Futyan, D., Gutermann, P., Maxted, P. F. L., Borsato, L., Collins, K. A., Gomes da Silva, J., Gómez Maqueo Chew, Y., Hooton, M. J., Lendl, M., Parviainen, H., Salmon, S., Schanche, N., Serrano, L. M., Sousa, S. G., Tuson, A., Ulmer-Moll, S., Van Grootel, V., Wells, R. D., Wilson, T. G., Alibert, Y., Alonso, R., Anglada, G., Asquier, J., Barrado y Navascues, D., Baumjohann, W., Beck, T., Benz, W., Biondi, F., Bonfils, X., Bouchy, F., Brandeker, A., Broeg, C., Bárczy, T., Barros, S. C. C., Cabrera, J., Charnoz, S., Collier Cameron, A., Csizmadia, S., Davies, M. B., Deleuil, M., Delrez, L., Demory, B. O., Ehrenreich, D., Erikson, A., Fossati, L., Fridlund, M., Gillon, M., Gömez-Munoz, M. A., Güdel, M., Heng, K., Hoyer, S., Isaak, K. G., Kiss, L., Laskar, J., Lecavelier des Etangs, A., Lovis, C., Magrin, D., Malavolta, L., McCormac, J., Nascimbeni, V., Olofsson, G., Ottensamer, R., Pagano, I., Pallé, E., Peter, G., Piazza, D., Piotto, G., Pollacco, D., Queloz, D., Ragazzoni, R., Rando, N., Rauer, H., Reimers, C., Ribas, I., Demangeon, O. D. S., Smith, A. M. S., Sabin, L., Santos, N., Scandariato, G., Schroffenegger, U., Schwarz, R. P., Shporer, A., Simon, A. E., Steller, M., Szabó, G. M., Ségransan, D., Thomas, N., Udry, S., Walter, I., and Walton, N. (2022). Uncovering the true periods of the young sub-Neptunes orbiting TOI-2076. *A&A*, 664:A156.

Pepe, F., Cristiani, S., Rebolo, R., Santos, N. C., Dekker, H., Cabral, A., Di Marcantonio, P., Figueira, P., Lo Curto, G., Lovis, C., Mayor, M., Mégevand, D., Molaro, P., Riva, M., Zapatero Osorio, M. R., Amate, M., Manescau, A., Pasquini, L., Zerbi, F. M., Adibekyan, V., Abreu, M., Affolter, M., Alibert, Y., Aliverti, M., Allart, R., Allende Prieto, C., Álvarez, D., Alves, D., Avila, G., Baldini, V., Bandy, T., Barros, S. C. C., Benz, W., Bianco, A., Borsa, F., Bourrier, V., Bouchy, F., Broeg, C., Calderone, G., Cirami, R., Coelho, J., Conconi, P., Coretti, I., Cumani, C., Cupani, G., D'Odorico, V., Damasso, M., Deiries, S., Delabre, B., Demangeon, O. D. S., Dumusque, X., Ehrenreich, D., Faria, J. P., Fragoso, A., Genolet, L., Genoni, M., Génova Santos, R., González Hernández, J. I., Hughes, I., Iwert, O., Kerber, F., Knudstrup, J., Landoni, M., Lavie, B., Lillo-Box, J., Lizon, J. L., Maire, C., Martins, C. J. A. P., Mehner, A., Micela, G., Modigliani, A., Monteiro, M. A., Monteiro, M. J. P. F. G., Moschetti, M., Murphy, M. T., Nunes, N., Oggioni, L., Oliveira, A., Oshagh, M., Pallé, E., Pariani, G., Poretti, E., Rasilla, J. L., Rebordão, J., Redaelli, E. M., Santana Tschudi, S., Santin, P., Santos, P., Ségransan, D., Schmidt, T. M., Segovia, A., Sosnowska, D., Sozzetti, A., Sousa, S. G., Spanò, P., Suárez Mascareño, A., Tabernero, H., Tenegi, F., Udry, S., and Zanutta, A. (2021). ESPRESSO at VLT. On-sky performance and first results. , 645:A96.

Pepper, J., Pogge, R. W., DePoy, D. L., Marshall, J. L., Stanek, K. Z., Stutz, A. M., Poindexter, S., Siverd, R., O'Brien, T. P., Trueblood, M., and Trueblood, P. (2007). The Kilodegree Extremely

Little Telescope (KELT): A Small Robotic Telescope for Large-Area Synoptic Surveys. *PASP*, 119(858):923–935.

Petigura, E. (2015). Prevalence of Earth-size Planets Orbiting Sun-like Stars. *arXiv e-prints*, page arXiv:1510.03902.

Petrovich, C., Muñoz, D. J., Kratter, K. M., and Malhotra, R. (2020). A Disk-driven Resonance as the Origin of High Inclinations of Close-in Planets. *ApJL*, 902(1):L5.

Rasio, F. A. and Ford, E. B. (1996). Dynamical instabilities and the formation of extrasolar planetary systems. *Science*, 274:954–956.

Ricker, G. R., Winn, J. N., Vanderspek, R., Latham, D. W., Bakos, G. Á., Bean, J. L., Berta-Thompson, Z. K., Brown, T. M., Buchhave, L., Butler, N. R., Butler, R. P., Chaplin, W. J., Charbonneau, D., Christensen-Dalsgaard, J., Clampin, M., Deming, D., Doty, J., De Lee, N., Dressing, C., Dunham, E. W., Endl, M., Fressin, F., Ge, J., Henning, T., Holman, M. J., Howard, A. W., Ida, S., Jenkins, J. M., Jernigan, G., Johnson, J. A., Kaltenegger, L., Kawai, N., Kjeldsen, H., Laughlin, G., Levine, A. M., Lin, D., Lissauer, J. J., MacQueen, P., Marcy, G., McCullough, P. R., Morton, T. D., Narita, N., Paegert, M., Palle, E., Pepe, F., Pepper, J., Quirrenbach, A., Rinehart, S. A., Sasselov, D., Sato, B., Seager, S., Sozzetti, A., Stassun, K. G., Sullivan, P., Szentgyorgyi, A., Torres, G., Udry, S., and Villasenor, J. (2015). Transiting Exoplanet Survey Satellite (TESS). *JATIS*, 1:014003.

Robertson, P., Anderson, T., Stefansson, G., Hearty, F. R., Monson, A., Mahadevan, S., Blakeslee, S., Bender, C., Ninan, J. P., Conran, D., Levi, E., Lubar, E., Cole, A., Dykhouse, A., Kanodia, S., Nitroy, C., Smolsky, J., Tuggle, D., Blank, B., Nelson, M., Blake, C., Halverson, S., Henderson, C., Kaplan, K. F., Li, D., Logsdon, S. E., McElwain, M. W., Rajagopal, J., Ramsey, L. W., Roy, A., Schwab, C., Terrien, R., and Wright, J. T. (2019). Ultrastable environment control for the NEID spectrometer: design and performance demonstration. *Journal of Astronomical Telescopes, Instruments, and Systems*, 5:015003.

Rossiter, R. A. (1924). On the detection of an effect of rotation during eclipse in the velocity of the brigher component of beta Lyrae, and on the constancy of velocity of this system. *ApJ*, 60.

Rubenzahl, R. A., Dai, F., Howard, A. W., Chontos, A., Giacalone, S., Lubin, J., Rosenthal, L. J., Isaacson, H., Batalha, N. M., Crossfield, I. J. M., Dressing, C., Fulton, B., Huber, D., Kane, S. R., Petigura, E. A., Robertson, P., Roy, A., Weiss, L. M., Beard, C., Hill, M. L., Mayo, A., Mocnik, T., Murphy, J. M. A., and Scarsdale, N. (2021). The TESS-Keck Survey. IV. A Retrograde, Polar Orbit for the Ultra-low-density, Hot Super-Neptune WASP-107b. *AJ*, 161(3):119.

Sanchis-Ojeda, R., Winn, J. N., Marcy, G. W., Howard, A. W., Isaacson, H., Johnson, J. A., Torres, G., Albrecht, S., Campante, T. L., Chaplin, W. J., Davies, G. R., Lund, M. N., Carter, J. A., Dawson, R. I., Buchhave, L. A., Everett, M. E., Fischer, D. A., Geary, J. C., Gilliland, R. L., Horch, E. P., Howell, S. B., and Latham, D. W. (2013). KEPLER-63b: A GIANT PLANET IN a POLAR ORBIT AROUND a YOUNG SUN-LIKE STAR. *The Astrophysical Journal*, 775(1):54.

Sasaki, S. and Suto, Y. (2021). Disentangling the stellar inclination of transiting planetary systems: Fully analytic approach to the Rossiter-McLaughlin effect incorporating the stellar differential rotation. *PASJ*, 73(6):1656–1668.

Schwab, C., Rakich, A., Gong, Q., Mahadevan, S., Halverson, S. P., Roy, A., Terrien, R. C., Robertson, P. M., Hearty, F. R., Levi, E. I., Monson, A. J., Wright, J. T., McElwain, M. W., Bender, C. F., Blake, C. H., Stürmer, J., Gurevich, Y. V., Chakraborty, A., and Ramsey, L. W. (2016). Design of NEID, an extreme precision Doppler spectrograph for WIYN. volume 9908 of *Proc. SPIE*, page 99087H.

Seifahrt, A., Stürmer, J., Bean, J. L., and Schwab, C. (2018). Maroon-x: A radial velocity spectrograph for the gemini observatory.

Southworth, J. (2011). Homogeneous studies of transiting extrasolar planets - IV. Thirty systems with space-based light curves. *MNRAS*, 417:2166–2196.

Speagle, J. S. (2020). DYNESTY: a dynamic nested sampling package for estimating Bayesian posteriors and evidences. *MNRAS*, 493(3):3132–3158.

Stefansson, G., Mahadevan, S., Hebb, L., Wisniewski, J., Huehnerhoff, J., Morris, B., Halverson, S., Zhao, M., Wright, J., O'rourke, J., Knutson, H., Hawley, S., Kanodia, S., Li, Y., Hagen, L. M. Z., Liu, L. J., Beatty, T., Bender, C., Robertson, P., Dembicky, J., Gray, C., Ketzeback, W., McMillan, R., and Rudyk, T. (2017). Toward Space-like Photometric Precision from the Ground with Beam-shaping Diffusers. *ApJ*, 848:9.

Stefansson, G., Mahadevan, S., Maney, M., Ninan, J. P., Robertson, P., Rajagopal, J., Haase, F., Allen, L., Ford, E. B., Winn, J., Wolfgang, A., Dawson, R. I., Wisniewski, J., Bender, C. F., Cañas, C., Cochran, W., Diddams, S. A., Fredrick, C., Halverson, S., Hearty, F., Hebb, L., Kanodia, S., Levi, E., Metcalf, A. J., Monson, A., Ramsey, L., Roy, A., Schwab, C., Terrien, R., and Wright, J. T. (2020). The Habitable Zone Planet Finder Reveals a High Mass and Low Obliquity for the Young Neptune K2-25b. *AJ*, 160(4):192.

Stefánsson, G., Mahadevan, S., Petrovich, C., Winn, J. N., Kanodia, S., Millholland, S. C., Maney, M., Cañas, C. I., Wisniewski, J., Robertson, P., Ninan, J. P., Ford, E. B., Bender, C. F., Blake, C. H., Cegla, H., Cochran, W. D., Diddams, S. A., Dong, J., Endl, M., Fredrick, C., Halverson, S., Hearty, F., Hebb, L., Hirano, T., Lin, A. S. J., Logsdon, S. E., Lubar, E., McElwain, M. W., Metcalf, A. J., Monson, A., Rajagopal, J., Ramsey, L. W., Roy, A., Schwab, C., Schweiker, H., Terrien, R. C., and Wright, J. T. (2022). The Warm Neptune GJ 3470b Has a Polar Orbit. *ApJL*, 931(2):L15.

Team, T. L. (2019). The luvoir mission concept study final report.

Winn, J. N., Johnson, J. A., Howard, A. W., Marcy, G. W., Isaacson, H., Shporer, A., Bakos, G. Á., Hartman, J. D., and Albrecht, S. (2010). The Oblique Orbit of the Super-Neptune HAT-P-11b. *ApJL*, 723(2):L223–L227.

Wirth, C. P., Zhou, G., Quinn, S. N., Mann, A. W., Bouma, L. G., Latham, D. W., Teske, J. K., Wang, S. X., Shectman, S. A., Butler, R. P., and Crane, J. D. (2021). Toi-942b: A prograde neptune in a 60 myr old multi-transiting system*. *ApJL*, 917(2):L34.

Wright, J. T. and Eastman, J. D. (2014). Barycentric Corrections at 1 cm s^{-1} for Precise Doppler Velocities. *PASP*, 126:838.

Yee, S. W., Petigura, E. A., and von Braun, K. (2017). Precision Stellar Characterization of FGKM Stars using an Empirical Spectral Library. *ApJ*, 836:77.

Zechmeister, M., Reiners, A., Amado, P. J., Azzaro, M., Bauer, F. F., Béjar, V. J. S., Caballero, J. A., Guenther, E. W., Hagen, H.-J., Jeffers, S. V., Kaminski, A., Kürster, M., Launhardt, R., Montes, D., Morales, J. C., Quirrenbach, A., Reffert, S., Ribas, I., Seifert, W., Tal-Or, L., and Wolthoff, V. (2018). Spectrum radial velocity analyser (SERVAL). High-precision radial velocities and two alternative spectral indicators. *A&A*, 609:A12.

Zhang, M., Knutson, H. A., Dai, F., Wang, L., Ricker, G. R., Schwarz, R. P., Mann, C., and Collins, K. (2023). Detection of Atmospheric Escape from Four Young Mini-Neptunes. *AJ*, 165(2):62.

Robert C. Frazier

robertcf300@gmail.com | rcf5201@psu.edu
LinkedIn
Personal Site

EDUCATION

The Pennsylvania State University — University Park, PA
Eberly College of Science, Schreyer Honors College — August 2019 - May 2023
Bachelor of Science in Astronomy and Astrophysics (Graduate Option) — Magna Cum Laude
Bachelor of Science in Physics (General Option) — Dean's List 7/7 semesters
Minor in Mathematics

PERSONAL EXPERIENCE

The Pennsylvania State University — University Park, PA
Research Assistant/Conducting Schreyer Honors College Thesis Research — March 2022 - Present

- Worked on characterization of exoplanet architecture via analysis of radial velocity data and the Rossiter-McLaughlin effect.
- Working on Honors Thesis: "Exploration of Obliquity Techniques on Warm Neptunes"

The Pennsylvania State University — University Park, PA
Research Assistant — May 2021 - October 2021

- Developing radio interferometry imaging Python package "MPoL." Improved accessibility features through tutorials and optimized the resource usage and run time of the package.

The Pennsylvania State University — University Park, PA
Learning Assistant — August 2020 - May 2021

- Instructed and guided students in intro-level physics-for-majors class's office hours and exam reviews.
- Assisted during lecture and instructed groups during the lab period; improved students' understanding and grades
- Graded weekly assignments and quizzes.

Upper Dublin School District — Fort Washington, PA
Internship with Science Curriculum Director/Planetarium Director — May 2019 - June 2019

- Participated in evaluation and curriculum meetings. Helped with curriculum organization.
- Educated and fostered an interest in science in classes of all ages through planetarium programs and presentations throughout the school district.

PUBLICATIONS, PRESENTATIONS, SOFTWARE

Frazier, R., Stefansson, G., Mahadevan, S. et al. 2022, (ApJL)
NEID Reveals that The Young Warm Neptune TOI 2076b Has a Low Obliquity

Zawadzki, B. (including Frazier) et al. 2022, AAS Journals (in review)
Regularized Maximum Likelihood Techniques for ALMA Observations

Czekala, I. (including Frazier) et al. 2021
MPoL-dev/MPoL: v0.1.1

PhysCon 2022 Finalist Presenter and APS Mid-Atlantic Meeting Poster Presentation
NEID Reveals that The Young Warm Neptune TOI 2076b Has a Low Obliquity

INVOLVEMENT

Society of Physics Students (SPS) August 2019 - present

- President for 22-23 Year (Plan and run meetings, outings, events, and coordinate all officers)
- Vice President for 21-22 Year (Ran outreach events, outings, and general meetings)
    - Directed and wrote “Magic Show” physics outreach play for 200+ visitors
- Buildmaster for 20-21 Year (Planned and prepared physics related builds)

Physics and Astronomy for Women+ (PAW+) August 2022 - present

- Web Chair for 22-23 Year (Maintain and update website)

PSU Conference for Undergraduate Women in Physics Planning Committee June 2022 - present

- Created and update website for event, gathered information and resources to be displayed on it
- Contacted all PA and western VA SPS chapters to invite to event in role as SPS President

APS IDEA Team March 2022 - present

- Work to change the climate in the Physics department and promote diversity, equity, and inclusion.

APS Climate Site Visit Team March 2022 - present

- Gather information and provide feedback and insight from undergrad level.

PHROTH August 2021 - April 2022

- Writer for PHROTH, Penn State satire newspaper and magazine

Students of Shield August 2019 - April 2022

AWARDS AND HONORS

Mercedes T. Richards Memorial Scholarship (PSU-Astronomy) Awarded 2022-2023

John and Elizabeth Holmes Teas Scholarship (PSU-Physics) Awarded 2021-2023

Sigma Pi Sigma Inducted April 2021

The President’s Freshman Award (PSU) Awarded 2020

Braddock Scholarship (PSU-Eberly College of Science) Awarded 2019-2023

RELEVANT COURSEWORK

- Planets and Planetary Systems
- Topics in Planetary Science
- Electronics for Scientists
- Theoretical Mechanics
- Observational Astronomy Lab
- Thermal Physics

TECHNICAL SKILLS AND CERTIFICATE

- Languages: Python (w/ Jupyter and VSCode) , Wolfram Language (w/ Mathematica)
- OS and Software: Linux and Windows. Office/Google Suite, AstroImageJ, LaTeX, Git
- Math through ODEs and PDEs, linear algebra, multivariable/vector calculus, advanced statistics
- Responsible Conduct of Research, Certificate of Completion
    - CITI Program